Synaptic activity-induced glycolysis supports neurite growth

Marc Segarra-Mondejar[1, 2], Sergi Casellas-Díaz[1, 2], Marina Ramiro-Pareta[1, 3], Claudia Müller-Sánchez[1], Alejandro Martorell-Riera[1, 6], Ismaïl Hermelo[1, 7], Manuel Reina[1], Julián Aragonés[4, 5], Ofelia M. Martínez-Estrada[1, 3], Francesc X. Soriano[1, 2]*

1 Celltec-UB, Department of Cell Biology, Physiology and Immunology

2 Institute of Neurosciences

3 Institute of Biomedicine

University of Barcelona, 08028 Barcelona, Spain

4 Research Unit, Hospital of La Princesa, Research Institute Princesa, Autonomous University of Madrid, 28009 Madrid, Spain

5 CIBER de Enfermedades Cardiovasculares, Carlos III Health Institute, Madrid, Spain

6 Present address: Department of Biological Chemistry, David Geffen School of Medicine at University of California Los Angeles, Los Angeles, CA 90095, USA.

7 Present address: BioMediTech, University of Tampere, 33520 Tampere, Finland

* Correspondence: f.x.soriano@ub.edu

Running title: Glycolysis is necessary for neurite growth

Abstract.

The formation of neurites is an important process affecting the cognitive abilities of an organism. Neurite growth requires the addition of new membranes, but the metabolic remodeling necessary to supply lipids for membrane expansion is poorly understood. Here, we show that synaptic activity, one of the most important inducers of neurite growth, transcriptionally regulates the expression of neuronal glucose transporter Glut3 and rate-limiting enzymes of glycolysis, resulting in enhanced glucose uptake and metabolism that is partly used for lipid synthesis. Mechanistically, CREB regulates the expression of Glut3 and Siah2, the latter and LDH activity promoting the normoxic stabilization of HIF-1α that regulates the expression of rate-limiting genes of glycolysis. The expression of dominant-negative HIF-1α or Glut3 knockdown blocks activity-dependent neurite growth *in vitro* while pharmacological inhibition of the glycolysis and specific ablation of HIF-1α in early postnatal mice impairs the neurite architecture. These results suggest that the manipulation of neuronal glucose metabolism could be used to treat some brain developmental disorders.

Key words: HIF-1α/ Siah2/ glycolysis/ synaptic activity-mediated transcription/ neurite growth

Introduction.

Early postnatal brain development is characterized by the massive outgrowth of dendrites and axons (Wong & Ghosh, 2002) (Silbereis et al). Among the different mechanisms affecting dendritic development, signaling from afferents is particularly important for dendritic growth (Groc et al, 2002; Konur & Ghosh; Rajan & Cline, 1998; Wong & Ghosh, 2002). The most active phase of dendritic growth in the rat cerebral cortex is concurrent with the time of afferent innervations (Konur & Ghosh; Wong & Ghosh, 2002). Moreover, blocking neuronal activity in vivo alters dendritic development (Groc et al, 2002; Rajan & Cline, 1998), while increased neuronal activity by exposure to an enriched environment positively influences dendritic growth (Faherty et al, 2003).

Activity-mediated calcium influx activates signaling events that influence dendritic architecture, modifiying cytoskeleton and activating transcriptional programs (Puram & Bonni, 2013; Wong & Ghosh, 2002). Several transcription factors and co-activators have been described to promote dendritic growth (Puram & Bonni, 2013), such as CREB, a transcription factor strongly activated by synaptic activity. In addition to its roles in cell survival and synaptic function, CREB is one of the most important transcription factors mediating activity-dependent dendritic morphogenesis in mammalian brain neurons (Lonze & Ginty; Puram & Bonni, 2013). Activation of CREB in cortical neurons induces dendritic growth and arborization, with dominant negative CREB suppressing activity-dependent neurite growth (Redmond et al). Furthermore, CREB knockout mice show impaired axonal growth and projections (Lonze et al). Despite the well-known function of CREB in regulating dendritic development, its target genes are not yet completely known.

Neurite growth requires cytoskeletal reorganization and cell membrane extension. The latter requiring a supply of lipids. Given the impermeable nature of the blood brain barrier (BBB)

most plasma lipoproteins cannot cross the BBB and lipids need to be synthesized in the brain. Studies investigating the incorporation of radiolabeled glycerol into lipids and their transport indicate that the bulk of lipid synthesis occurs in the cell body of neurons, with the lipids then exported in vesicles to the axon and dendrites for membrane expansion (Goldberg, 2003; Pfenninger, 2009). However, little is known on where the precursors necessary for lipid synthesis come from. The intermediates of glycolysis serve as lipid precursors (Vander Heiden et al, 2009). Dihydroxyacetone phosphate (DHAP) is converted by glycerol-3-phosphate dehydrogenase 1 (GPD1) into glycerol-3-phosphate, which is then used for synthesizing glycerol-backbone lipids. Pyruvate, the end product of glycolysis, is transported to the mitochondria where it enters the tricarboxylic acid (TCA) cycle as citrate and is further metabolized or exported to the cytoplasm to be broken down by ATP-citrate lyase (ACLY) into oxaloacetate and acetyl-CoA, which serves as a precursor in lipid biosynthesis. Meta-analysis of brain and glucose consumption demonstrates that aerobic glycolysis increases in the human brain when synaptic growth rates are highest, suggesting that glycolysis provides biosynthetic support for neurite growth (Goyal et al, 2014). However, it is unclear whether glycolysis is regulated by neuritogenic cues or is needed for neurite growth.

Hypoxia inducible factor 1 (HIF-1) is a transcription factor regulating adaptive responses to hypoxia. It occurs as heterodimer composed of an unstable HIF-1α and a stable HIF-1β (also known as ARNT). The heterodimer binds hypoxia response elements (HRE) on target genes, which includes those associated with glucose transport and glycolysis genes, among others (Denko, 2008; Semenza et al, 1994). Normally, HIF-1α is ubiquitinated and degraded in normoxic conditions. Hydroxylation of Pro- 402 and Pro-564 by prolyl hydroxylases (PHD) in the oxygen-dependent degradation domain (ODD) of human HIF-1α promotes interaction with the von Hippel-Lindau ubiquitin ligase complex (VHL) which targets HIF-1α for proteolysis (Ivan et al, 2001; Jaakkola et al, 2001; Maxwell et al, 1999). Another regulatory element of the PHD/VHL pathway is the E3 ubiquitin ligase Siah2, which contributes to HIF-1α stabilization (Li

et al, 2017; Nakayama et al, 2004). Despite its generally short half-life in normoxia, HIF-1α can be stabilized in normoxia by growth factors, metabolite accumulation, the expression of oncogenes or ROS production (Denko, 2008).

Although much is known on the molecular mechanisms mediating cytoskeletal remodeling and lipid transport to induce neurite growth, little is known about the metabolic adaptations required for neuronal membrane extension. Here, we show CREB activation by synaptic activity induces the expression of the glucose transporter Glut3 and promotes Siah2-mediated stabilization of HIF-1α that upregulates the expression of glycolysis genes. As a consequence, glucose metabolism is enhanced and part of it is used to provide the lipid precursors necessary for neurite growth.

Results

Glucose metabolism is necessary for activity-dependent neurite outgrowth.

Neuronal activity promotes neurite growth which requires a supply of lipids to enlarge membranes. Accordingly, using an established method of network disinhibition to enhance synaptic activity by applying the GABAA receptor antagonist bicuculline (Bic) and the K^+ channel antagonist 4-aminopyridine (4AP) (Hardingham et al, 2001), we observed that active neurons have increased levels of FASN and ACLY (Appendix Fig. S1A-C), two key enzymes for the novo lipid synthesis.

Glucose-derived acetyl-CoA is the main precursor for lipid biosynthesis (Divakaruni et al, 2017; Pietrocola et al, 2015). Thus, it was analyzed incorporation of radioactively labeled glucose into lipids in neurons that have experienced an episode of synaptic activity. After 48 hours of stimulation, active neurons showed increased glucose incorporation into lipids (Fig. 1A). This was impaired by knockdown of the glycolytic enzyme GPI (Fig. 1B and Appendix Fig. S1D). Glutamine metabolism is another major source of lipogenic acetyl-CoA (Pietrocola et al, 2015),

however synaptic activity did not increase glutamine incorporation into lipids (Appendix Fig. S1E).

One molecule of glucose is converted to two molecules of pyruvate during glycolysis. Pyruvate enters the mitochondria, where it is decarboxylated to produce acetyl-CoA that then conjugates with oxaloacetate to produce citrate. Citrate can be further metabolized in the TCA cycle or exported to the cytoplasm, where it is converted into acetyl-CoA by ACLY to be used for fatty acid synthesis. Total and cytosolic acetyl-CoA levels were also increased in active neurons (Fig. 1C and D), but not CoA levels (Appendix Fig. S1F), which was not observed when glycolysis was inhibited with 2-deoxy-D-glucose (Fig 1E), indicating a major role of glucose as a source of the increased amounts of acetyl-CoA. In agreement, knockdown of ACLY blocked activity-dependent enhanced glucose incorporation into lipids (Fig. 1F and Appendix Fig. S1G and S1H).

In accordance with the need of glucose-derived lipid production to enlarge membranes for neurite growth, knockdown of Glut3 (Fig. 1G and H), the main glucose transporter in neurons, inhibition of glucose metabolism with 2-DG (Appendix Fig. S1I), or knockdown of ACLY (Appendix Fig. S1J) abolished activity-mediated neurite growth which at this developmental stage represents axonal growth.

Synaptic activity stimulates neuronal glucose uptake and metabolism at the transcriptional level.

To investigate whether increased acetyl-CoA levels correlated with increased glucose uptake and metabolism, neurons were stimulated for 24 hours with Bic+4AP, and washed for 30 minutes to allow restoration of ion gradients before analyzing glucose uptake. Bic+4AP washing effectively blocked burst firing (Appendix Fig. S2A and B). It was found that neurons that had experienced synaptic activity increased their glucose uptake (Fig. 2A and Appendix Fig. S2C). Glycolysis-produced pyruvate is partially metabolized into lactate in a reaction that

regenerates NAD^+ that is necessary for glycolysis to continue. Glycolysis is the main source of lactate, accounting for 82-90% on different types of cells (Zhang et al, 2017). Thus, lactate release into the medium is a commonly used surrogate of glycolytic flux (TeSlaa & Teitell, 2014). Active neurons released 75% more lactate than resting ones (Fig. 2B). This was not due to the hyperglycemic medium used in this study, since culturing the neurons with physiological glucose concentration in rat brain (2.4 mM; (Silver & Erecinska, 1994)) produced similar lactate release (Appendix Fig. S2D). In another approach to demonstrate increased glycolysis in active neurons, neurons were stimulated for 24 hours and washed for 30 minutes, to allow restoration of ionic gradients, before uncoupling the mitochondria with CCCP for 30 minutes. This drastically reduced ATP levels, which were less reduced in the stimulated neurons than unstimulated ones, but only when glucose was present in the medium (Fig. 2C), indicating that the increased glycolysis in active neurons can supply more ATP than in resting ones when the mitochondria are not functional.

Synaptic activity has been shown to mediate Glut3 translocation to the membrane (Ferreira et al, 2011). Moreover, synaptic activity is a potent regulator of gene expression programs (Bading, 2013; Greer & Greenberg, 2008). Thus, we aimed to determine whether activity-mediated glycolysis induction was mediated at the transcriptional or posttranslational level. Cycloheximide was used to inhibit mRNA translation. If glucose metabolism induction was mainly due to posttranslational modifications, the increase in glucose metabolism would not be affected by cycloheximide treatment; it would be affected by cycloheximide if de novo protein synthesis was involved. We found that cycloheximide abolished the glucose metabolism induced by synaptic activity, which was established by measuring lactate release (Fig. 2B). This was not consequence of reduced neuronal viability since cycloheximide treatment did not affect viability (Appendix Fig. S2E). Next, we used qPCR to analyze the expression of Glut3, the main glucose transporter in neurons; HK2, PFK and PKM, the three regulating enzymes of the glycolysis; and PFKFB3, which produces fructose-2,6-bisphosphate, a

potent allosteric activator of PFK. There was an increase in the expression of all these genes except PFK (Fig. 2D). Strikingly, Glut3 showed a different expression pattern to these associated with glycolysis. Along with the increased mRNA levels, synaptic activity induced the protein expression of these genes (Fig. 2E and F). Interestingly, treatment of neurons with BDNF, a neurotrophic factor that induces neurite growth (Park & Poo, 2013), also induced the expression of glucose metabolism genes, as well as increased glucose uptake and lactate release (Appendix Fig. S2F-H), although it cannot be excluded an indirect effect due to BDNF-induced enhanced neuronal activity (Li et al, 1998).

Glial and neuronal metabolism is coupled (Bélanger et al). Around 2% of our primary cortical neuron cultures were glial cells (Appendix Fig. S2I and J). Neuronal glucose uptake experiments were analyzed by cell imaging, but the lactate release and ATP production experiments were performed using the mixed cultures. Thus, we could not rule out the possibility that activity-dependent enhanced glycolysis occurred in the glial cells rather than neurons. To clarify this, we used two approaches. The mitosis inhibitor AraC is used in our cortical cultures to block glial proliferation. In a first approach, we prepared parallel cortical cultures that were treated with AraC or not to obtain cultures with different proportions of glial cells (Appendix Fig. S2I and J). If the stimulation-mediated increase in lactate release was due to changes in gene expression in glial cells rather than neurons, modifying the abundance of glial cells in the co-culture would elicit a corresponding increase in lactate release after stimulation. Although cultures not treated with AraC had around tenfold more astrocytes than AraC treated ones, these two types of cultures showed the same degree of lactate release when stimulated, confirming that the enhanced glucose metabolism, and, consequently the expression of glucose metabolism genes when stimulated occurred in neurons rather than astrocytes (Appendix Fig. S2K). In the second approach, we used pure astrocyte cultures. Astrocytes express functional BDNF receptors (Ohira et al, 2005; Rose et al, 2003), however BDNF did not increased lactate release in pure astrocyte cultures like it did in neuronal cultures (Appendix

Fig. S2H and 2L). Thus, enhancement of glucose metabolism takes place in neurons when stimulated with neurite growth inducers.

Activity-dependent induction of glycolysis genes depends on HIF-1a stabilization.

Next we investigated the transcription factor responsible for the induction of activity-mediated glucose metabolism genes. HIF-1α is a transcription factor that stimulates glycolysis by transactivating the genes involved in intracellular glucose transport and glycolysis (Denko, 2008; Semenza et al, 1994). Although HIF-1α is typically unstable in normoxia, certain conditions enable its stabilization in normoxic conditions (Denko, 2008). Thus, HIF-1α could be responsible for inducing glucose metabolism genes. We observed HIF-1α stabilization in active and BDNF treated neurons (Figs. 3A, 3B, and EV1A-C), but not HIF-2α (Fig. EV1E and F), that correlated with increased HIF-1α transcriptional activation (Fig. 3C). Overexpression of HIF-DN, a dominant negative form of HIF-1α (HIF-DN) formed by the DNA binding domain of HIF-1α and lacking the prolyl hydroxylase and transactivation regions, completely blocked activity-mediated transcriptional activation of HIF-1α (Fig. 3C). Transduction with AAV-HIF-DN blocked activity-dependent induction of glycolysis genes, but had no effect on Glut3 gene expression (Fig. 3D). This was not completely surprising because the pattern of Glut3 expression was different to that of the glycolysis genes (Fig. 2D). All together, these results indicate that the activity-dependent induction of glycolysis genes depends on HIF-1α. Consequently, the activity-mediated lactate release and glucose incorporation into lipids was reduced in HIF-DN expressing neurons (Fig. 3E and F).

HIF-1α is stabilized by Siah2 and LDH activity.

HIF-1α regulation is mainly mediated by proteosomal degradation in normoxia. Hydroxylation of prolynes in the ODD domain of HIF-1α by PHDs promotes HIF-1α proteolysis (Ivan et al, 2001; Jaakkola et al, 2001; Maxwell et al, 1999). We studied whether synaptic activity

decreased PHD activity. Neurons were transfected with a plasmid expressing firefly luciferase fused to the oxygen-dependent degradation domain of HIF-1α (ODD-Luc). Synaptic activity resulted in increased luciferase activity in ODD-Luc, but not wild type firefly luciferase (Luc) transfected neurons (Fig. 4A and 4B), indicating reduction in PHD activity. Siah2 is an E3 ubiquitin ligase that promotes HIF-1α stabilization mainly by mediating proteasomal degradation of PHDs (Nakayama et al, 2004), although other mechanisms by which Siah2 promotes HIF-1α stabilization have been also described (Li et al, 2017). Siah2 mRNA and protein levels were induced by synaptic activity (Fig. 4C-E) and BDNF (Fig. EV1B and D and Appendix Fig. S3B), correlating with reduced PHD activity. While Siah1 is downregulated by synaptic activity (Appendix Fig. S3A). To confirm the role of Siah2 in activity-dependent HIF-1α stabilization, we knocked down (KD) Siah2 by transducing the neurons with two AAV expressing different shRNAs targeting Siah2. Siah2 KD neurons showed a strong reduction of activity-dependent HIF-1α accumulation (Fig. 4F-H and Appendix Fig. S3C-G). Next, we checked the expression levels of PHD in active neurons and surprisingly we observed no changes in PHD1, PHD3 and FIH, and increased expression of PHD2 (Appendix Fig. S3H and I). One alternative mechanism by which Siah2 could HIF-1α is mediating degradation of the enzymes of the OGDHC, OGDH and DLST (Burr et al, 2016; Intlekofer et al, 2017; Nadtochiy et al, 2016; Sun & Denko, 2014) , but we could not observe changes in protein levels of these enzymes (Appendix Fig. S3H and I). However, a central role of Siah2 upregulation in the activity-mediated enhanced glucose metabolism was further confirmed by showing that Siah2 KD blocked activity-mediated lactate release (Fig 4I) and glucose incorporation into lipids (Fig. 4J).

HIF-1α regulation is complex, with several regulators and mechanisms being involved. We tested whether other mechanisms different from the one mediated by Siah2 induction could participate as well in activity-mediated HIF-1α stabilization. HIF-1α is an O_2 sensitive transcription factor that mediates the primary response to hypoxic stress. Excessive O_2

consumption in active neurons could generate transitory hypoxia that mediates HIF-1α stabilization. However, the use of a hypoxia sensor probe did not show hypoxia generation by synaptic activity (Appendix Fig. S3J). Despite synaptic activity regulates a transcriptional program of defense against oxidative stress (Papadia et al, 2008), acute synaptic activity could boost mitochondrial metabolism and enhance ROS production which is involved in HIF-1α stabilization in normoxia, therefore we tested whether the use of antioxidants could block HIF-1α activation by synaptic activity, but it did not have any effect on activity-mediated HIF-1α stabilization (Appendix Fig. S3K and L). Increased HIF-1α levels in active neurons were not due to the transcriptional regulation of HIF-1α either (Appendix Fig. S3M). Both rise in pyruvate and lactate levels stabilize HIF-1α (Lu et al, 2002). We inhibited LDH with oxamate, which produces accumulation of pyruvate and reduces lactate release (Lu et al, 2002). Oxamate treatment blocked activity-mediated HIF-1α stabilization (Fig 4K and L). Since, both, Siah2 KD and LDH inhibition almost completely blocked activity-mediated HIF-1α stabilization they may be part of the same regulatory pathway.

Glut3 and Siah2 expression is regulated by CREB.

Since Glut3 expression in active neurons did not depend on HIF-1α activation, we explored which transcription factor could regulate it. CREB is a powerful regulator of synaptic activity-mediated gene expression (Bading, 2013; Greer & Greenberg, 2008), controls neurite outgrowth (Redmond et al) and is involved in metabolic regulation in different cell types (Altarejos & Montminy, 2011). CREB has been shown to regulate Glut3 expression (Rajakumar et al, 2004); thus, we tested whether CREB was involved in activity-mediated Glut3 expression. Transduction of neurons with AAV expressing a dominant negative CREB (A-CREB; (Ahn et al, 1998)) blocked activity-dependent Glut3 expression (Fig. 5A).

Given that Glut3 and Siah2 showed a similar pattern of mRNA expression following synaptic activity, a high activation after four hours with the decay at 24 hours (Fig. 2D and 4C), we

assessed whether Siah2 was also regulated by CREB. A-CREB blocked Siah2 induction (Fig. 5B-D) and, consequently, blocked the HIF-1α stabilization induced by synaptic activity (Fig. 5C and E). Furthermore, over-expression of the endogenous CREB inhibitor ICER (Molina et al, 1993) also blocked HIF-1α activity (Fig. 5F) but did not disturb the activity of MEF2 (Fig EV2A), an activity-dependent transcription factor (Greer & Greenberg, 2008). Forskolin, adenylyl cyclase activator and hence CREB activator, was sufficient to induce Siah2 expression and HIF-1α stabilization and activation (Fig. 5G-J). In agreement with an indirect CREB-dependent activation of HIF-1α via increased Siah2 expression, we observed that CREB activation preceded HIF-1α activation (Fig. 5K).

As expected, A-CREB expression blocked activity-dependent lactate release (Fig. 5L) and glucose incorporation into lipids (Fig. 5M). Forskolin also stimulated lactate release (Fig. EV2B) but had no effect on glucose incorporation into lipids (Fig. EV2C), in agreement with the fact that cAMP greatly potentiates neuritic growth in response to neurotrophic factors but does not promote growth by its own (Goldberg et al, 2002).

Defective glycolysis impairs neurite growth.

This and the previous results suggest that Siah2 and HIF-1α may be necessary for neurite growth through regulating glycolysis. Indeed, HIF-1α or Siah2 over-expression in DIV 3 immature cortical neurons increased neurite length (Fig 6A-C) that at this stage represents axonal growth (Dotti et al, 1988). While HIF-DN expression or Siah2 knockdown blocked activity-dependent neurite growth in DIV 10 cortical neurons (Fig. 6D-G).

The first three weeks after birth is when maximum neurite growth occurs in mice, being synaptic activity one of the effectors of this growth (Wong & Ghosh, 2002). In order to provide evidence about the *in vivo* role of glucose metabolism we administered PFKFB3 inhibitor 3PO

(Schoors et al, 2014) for 5 days to rat pups that were 8 days old. Golgi staining showed reduced complexity of neuritic arbors in the cortex of 3PO administered rats (Fig. 6H-I).

HIF-1α deletion in neural precursor cell progenitors leads to atrophy of the cerebral cortex, indicating an important role for HIF-1α in neuronal development in vivo (Tomita et al, 2003). Thus, we compared HIF-1α expression in the brains of mice that were 10 days and 3 months old. We observed a higher density of HIF-1α positive cells and increased protein levels in 10 day-old mice compared to 3 month-old mice (Fig. 6J and Fig. EV3A and B). Expression of HIF-1α in 10 day-old mice brain was highest in cortex, hippocampus and corpus callosum (Fig. EV3C). Dual staining reveled colocalization of HIF1α with the neuronal marker NeuN, and complete absence in astrocytes expressing GFAP (Fig. 6K).

In order to provide evidence about the in vivo role of HIF-1α in neurite growth, we deleted HIF-1α in tamoxifen inducible HIF-1α KO mice that were 3-5 days old, when gross anatomy of the brain resembles to that of the adult but is characterized by outgrowth of dendrites and axons. Once these animals reached adulthood (4-6 months), the neuronal architecture of the cortex of WT and HIF-1α KO mice was analyzed by Golgi staining, which showed reduced complexity of neuritic arbors in the KO mice (Fig. 6L and M). Interestingly, glucose metabolism is necessary for axonal growth in vitro with no effect on dendritic growth meanwhile in vivo the effect observed accounts mainly for dendritic growth. This possibly is due to the fact that at the developmental stage when neurites were analyzed in vitro dendrites are mostly stable and axons are still growing while postnatal dendrites are still growing. Taken together, our results indicate that induction of glucose metabolism in neurons is required for proper neuronal development regardless the neurons are in axonal or dendritic growth state.

Discussion.

Signaling from afferents plays an essential role in neurite growth (Groc et al, 2002; Rajan & Cline, 1998; Wong & Ghosh, 2002). Here, we show that activity-dependent neurite growth requires induction of glucose metabolism. Synaptic activity enhances glucose uptake and metabolism, some of which is diverted towards lipid synthesis that is required for cell membrane enlargement during outgrowth. The induction of glucose metabolism is mediated at the transcriptional level, CREB induces Glut3 and Siah2, the latter promoting the normoxic stabilization of HIF-1α that regulates the expression of the rate-limiting enzymes involved in glycolysis (Fig. 7).

Most of the glucose in the brain is oxidized to supply the large amounts of ATP required for maintaining membrane ion gradients and processes regulating to synaptic transmission (Harris et al; Magistretti & Allaman, 2015; Rangaraju et al). However, measurements of human brain glucose and oxygen consumption reveal that the total amount of glucose consumed is in excess of oxygen consumption (Goyal et al, 2014; Vaishnavi et al, 2010). The utilization of aerobic glycolysis in the human brain differs across the developmental stages, with 35% of glucose being consumed aerobically after birth that falls to 10-12% in adulthood (Goyal et al, 2014). This increased aerobic glycolysis during infancy correlates with the period of maximal neurite growth (Goyal et al, 2014; Silbereis et al, 2016). Neuronal differentiation in vitro show increased expression levels of Glut3 and glycolysis enzymes, with 2-DG treatment of DIV1 cortical neurons blocking differentiation (Agostini et al, 2016). These data agree with our findings that activity-dependent aerobic glycolysis is used to meet the biosynthetic requirements for neurite growth. Highly proliferative cancer cells rely on aerobic glycolysis, which it is known as the Warburg effect (Vander Heiden et al, 2009). Despite aerobic glycolysis being a less efficient way of generating ATP it confers advantages to cancer cells such as the production of intermediates that support cell growth and division (Vander Heiden et al, 2009). Although postmitotic neurons do not divide, they undergo massive growth during differentiation. A neurite with a diameter of 1 μm elongating 0.55 μm per day must expand its

surface at a rate of around 1μm^2 per minute to reach 250,000 μm^2 which is the typical neuron surface area, compared with 1,256 μm^2 membrane surface of a spherical cell with 20 μm diameter (Pfenninger, 2009).

Astrocytes and neurons are metabolically coupled. The astrocyte-neuron lactate shuttle (ANLS) hypothesis proposes that the lactate produced by astrocytes is released and taken up by neurons to produce energy (Pellerin & Magistretti, 1994). Although there is a lot of evidence supporting the ANLS there are also data that oppose this hypothesis (Dienel, 2017; Lundgaard et al, 2015; Patel et al, 2014; Pellerin & Magistretti, 2012). Here, we clearly demonstrate that synaptic activity boosts glucose uptake and metabolism in neurons, rather than glial cells, by upregulating Glut3 and glycolysis genes. Increasing the proportion of glial cells in our primary cultures did not result in increased lactate release after stimulation, neither BDNF treatment affected lactate release in astrocytes unlike the stimulatory effect in lactate release in neuronal cultures. Moreover, glucose uptake in neurons was observed by live-imaging, and HIF-1α activation measured with luciferase reporters is based in neuronal-specific transfection protocol which nearly the totality of transfected cells are neurons (Soriano et al, 2008). In accordance with our results, a very recent study (Bas-Orth et al, 2017) showed synaptic activity caused an up-regulation of glycolytic genes with the subsequent increase in glycolytic metabolism. Isolating neurons by FACS allowed the authors to conclude that the induction of glycolytic genes was produced in neurons. Despite strong evidence indicating that glucose metabolism is activated by synaptic activity in neurons, these results do not oppose the ANLS, but supports the notion that neurons take up and metabolize through glycolysis in certain conditions (Ashrafi et al, 2017; Díaz-García et al, 2017; Jang et al; Lundgaard et al, 2015; Zala et al). Cell division, migration and neurite growth require extraordinary levels of energy that would explain why the supply of energy in neurons is not limited to the astrocytic lactate during pre- and postnatal stages. This is also seen in the support of cholesterol synthesis in neurons by astrocytes, which can supply sufficient levels of cholesterol to adult neurons

unable to synthesize cholesterol, but cannot do so during the phase of maximal membrane growth (Fünfschilling et al, 2012).

Activity-mediated CREB activation plays a pivotal role in enhanced glucose metabolism. In neurons, CREB is a key transcription factor that regulates plasticity, cell survival and neurite growth (Bading, 2013; Greer & Greenberg; Lonze & Ginty, 2002; Redmond et al, 2002). In peripheral tissues, CREB has a major metabolic role, regulating glucose and lipid metabolism in insulin-sensitive tissues (Altarejos & Montminy, 2011). As previously described (Rajakumar et al, 2004), we observed CREB-mediated regulation of Glut3 gene expression, the main glucose transporter in neurons. In addition, CREB promoted Siah2 gene expression and, consequently, HIF-1α stabilization, which resulted in the increased gene expression of the rate-limiting enzymes involved in glycolysis. HIF-1α is best known as a transcription factor that mediates adaptation to hypoxia. Genes associated with glucose metabolism are the largest functional group regulated by HIF-1α (Denko, 2008; Semenza et al, 1994). HIF-1α KO leads to embryonic lethality at E11, producing cardiovascular and brain malformations (Iyer et al, 1998; Ryan et al, 1998). HIF-1α deletion in neuronal progenitors elicits cerebral cortex atrophy, defective brain development with fewer neural cells and impaired of spatial memory (Tomita et al, 2003) however HIF-1α deletion in mature neurons using CaMKII-CRE does not generate any evident major morphological defect (Helton et al, 2005). Here, we show that HIF-1α deletion in early postnatal mice, a period of maximal afferent innervations and neurite growth, disturbs neurite architecture in the adult.

HIF-1α activation is regulated at multiple levels. We observed that synaptic activity reduced PHD activity, while CREB upregulated the expression of the ubiquitin ligase Siah2, and that activity-dependent induction of Siah2 is necessary for stabilizing HIF-1α. Siah2 KO mice exhibit mild phenotypes and do not show obvious brain abnormalities (Frew et al, 2003). However, the presence of other Siah proteins (1a and 1b) may explain this lack of phenotype, given that

double Siah1a/2 KO animals show a more severe phenotype regarding HIF-1α activity than Siah2 KO mice (Nakayama et al, 2004). The first mechanism described by which Siah1 and 2 proteins stabilize HIF-1α was by promoting proteasomal degradation of PHDs (Nakayama et al, 2004). However, we could not detect reduction in PHDs after synaptic activity. HIF-1α is known to interact with more than one hundred proteins (Semenza, 2017), most of them regulating HIF-1α stability. Among the interacting proteins some of them have been shown to be targeted by Siah2, such as Polo-like kinase 3 (PLK3) that phosphorylates and destabilizes HIF-1α (Xu et al, 2010), and Siah2-mediated PLK3 degradation results in HIF-1α activation (Li et al, 2017). Sprouty2 promotes HIF-1α ubiquitination (Hicks & Patel, 2016), is regulated by Siah2 (Qi et al, 2008) and its downregulation promote axonal growth (Hausott et al, 2009; Hausott et al, 2012; Marvaldi et al, 2015), however the link between these three observations have not been established. We observed that both Siah2 knockdown or LDH inhibition almost completely blocked activity-dependent HIF-1α stabilization, what indicates that they may share a common regulatory pathway. Acid pH and LDH promotes the noncanonical conversion of 2-oxoglutarate to L-2-HG which functions as a potent inhibitor of PHDs (Burr et al, 2016; Intlekofer et al, 2017; Nadtochiy et al, 2016). Disruption of OGDHC results in accumulation of oxoglutarate with the subsequent increase in L-2-HG and HIF-1α stabilization (Burr et al, 2016). Siah2 has been reported to disrupt OGDHC complex (Habelhah et al, 2004; Sun & Denko, 2014) but acute synaptic activity did not affect protein levels of OGDHC. Future studies will be aimed to understand the interrelationship between Siah2 and LDH to promote activity-mediated HIF-1α stabilization.

Disruption of dendritic development is the most consistent anatomical finding in mental retardation (Kaufmann & Moser, 2000). The role of abnormal cytoskeletal remodeling has been associated with mental retardation in some syndromes but further studies are required to determine how glucose metabolism is affected. Glut1 deficiency syndrome or chronic

hypoglycemia (congenital or early infantile) causes the syndrome of glycopenia which is characterized by seizures, developmental delay and mental retardation (Pascual et al, 2007). Here, we have showed that activity-mediated neurite growth requires enhanced glucose metabolism to supply lipids for membrane enlargement. Further studies are required to determine how glucose metabolism is affected in intellectual development disorders. Those studies could lead to the possibility of manipulating glucose metabolism to treat of some forms of intellectual development disorders.

Material and methods

Cell culture and stimulation

Cortical neurons from E21 Sprague Dawley rats were cultured as described previously (Martorell-Riera et al, 2015). See supplementary information.

HIF-1α gene inactivation in vivo

To study the in vivo role of HIF-1α in neuronal architecture, we used previously described HIF1α floxed UBC-CRE-ERT2 mice (Soro-Arnaiz et al, 2016). These mice ubiquitously express a tamoxifen-inducible CRE recombinase (cre-ERT2) that allows global inactivation of HIF-1α locus flanked by two LoxP sites upon 4OH-tamoxifen treatment. For HIF-1α gene inactivation, the newborn mice received tamoxifen via breast feeding from the mother. Weaning mothers were injected intraperitoneally with 4OH-tamoxifen daily for 5 days (2 mg/day) starting 3-5 days postpartum. After this period females were returned to a standard mouse diet. Once newborns reached adulthood (4-6 months) neuronal architecture was analyzed. Mice were kept under specific pathogen-free conditions at the animal facility at the Autonomous University of Madrid (UAM).

3PO administration

See supplementary information

Histology

See supplementary information

Transfection, plasmids and virus generation

Neurons were transfected at DIV8 using Lipofectamine 2000 (Invitrogen). Transfection efficiency was approximately 5 % which nearly the totality of transfected cells are neurons (Soriano et al, 2008).

Neurons were infected with rAAV at DIV4. Infection efficiencies were determined at DIV 10-11 by analyzing GFP fluorescence or immunocytochemical analysis and were observed to range from 70 to 85% of the viable neurons. See supplementary information

Neurite length measurement

Cortical neurons were transfected with a plasmid expressing GFP and neurons were fixed 48 hours later with 4% paraformaldehyde, permeabilized, blocked and incubated over-night at 4°C with anti-GFP antibody (1:750, A11122, Life Technologies). Antibody binding was visualized using a biotinylated secondary antibody (1:200, Jackson Immuno Research) and Cy3-conjugated streptavidin (1:500, Jackson Immuno Research). Preparations were mounted on VECTASHIELD Mounting Medium with DAPI (Vector Laboratories).

Images were taken blindly at 4X magnification using an Olympus BX61 microscope equipped with an Olympus DP70 camera. Neurites were manually traced and analyzed using Simple Neurite Tracer software (Longair et al, 2011).

Luciferase assays

Cells were transfected with firefly luciferase-based reporter plasmid along with a Renilla expressing vector (pTK-RL; Promega), together with, where relevant, an HIF-DN or A-CREB expression vector. Luciferase assays were performed using the Dual Glo Luciferase Assay system (Promega) with firefly luciferase-based reporter gene activity normalized to the Renilla control (pTK-RL plasmid), except the CMV-ODD-Luc and CMV-Luc experiments that were normalized to CMV-Renilla.

RNA isolation, RT-PCR and qPCR

RNA was isolated using an PureLink^{TM} RNA mini kit (Life Technologies). For qPCR, cDNA was synthesized from RNA using the SuperScript® III First-Strand Synthesis SuperMix (Life Technologies) following the manufacturer's instructions. qPCR was performed in a StepOne Real-Time PCR System (Applied Biosystem) using GoTaq qPCR Master Mix (Promega) according to the manufacturer's instructions. See supplementary information

Western blotting and antibodies

See supplementary information

Acetyl-CoA and CoA determination

Acetyl-CoA and CoA levels were measured using the Acetyl-Coenzyme A and CoA Assay Kits, respectively (Sigma). See supplementary information.

Glucose uptake measurements

The uptake of 2-[*N*-(7-nitrobenze-2-oxa-1, 3 diazol-4-yl) amino]-2 deoxy-glucose (2-NBDG, Life Technologies), a fluorescent glucose analog, was used to measure glucose transport. Cortical neurons were rinsed 3 times with phenol-red free SGG medium with reduced glucose concentration (0.5 mM) and incubated with 100 μM 2-NBDG in reduced glucose SGG medium for 30 minutes at 37ºC and 5% CO_2. Cultures were washed three times with phenol-red free

SGG medium to remove free 2-NBDG. Accumulation of intracellular 2-NBDG, measured using an excitation wavelength of 488 nm, was imaged under a Leica DMIRB microscope equipped with a Leica DFC 550 camera at 40× magnification. ROIs of the same surface were drawn in the soma and fluorescence intensity was analyzed using ImageJ (Schneider et al, 2012).

Imaging studies

Neurons were visualized using a TCS SP2 Leica confocal laser scanning microscope (Leica Lasertechnick GmbH, Mannheim, Germany) adapted to an inverted Leitz DMIRBE microscope at 37°C in a controlled 5% CO2 atmosphere (Life Imaging Services). Pictures were acquired using a 40× (1.25-0.75 NA) Leitz Plan-Apochromatic objective. Images were analyzed using ImageJ software.

Cytoplasmic Ca^{2+} was monitored with Fluo-4 (Life Technologies). Neurons were loaded 2 µM Fluo-4 for 45 min at room temperature in phenol-red free SGG medium with 10mM HEPES and 10mM glucose. After 3 washes with phenol-red free SGG medium, neurons were de-esterified for 30 min at room temperature, excited at 488 nm and emission captured with a 516-nm filter.

For hypoxia analysis, neurons were loaded with 10 µM Image-IT Hypoxia Reagent (Life Technologies) in HBSS medium, and placed in an incubator chamber attached to the microscope, which was flushed with 95% N2/5% CO2 at a flow rate of 20 l/min at 37°C for 30min. Non-hypoxic neurons were maintained in normoxic conditions during probe incubation. Neurons were excited at 490 nm, and emission was measured using a 610-nm filter.

Lactate measurement

The culture medium was filtered using 10K Amicon Ultra-0.5 mL centrifugal filters (EMD Millipore). Then, 50 µL of medium was incubated with 200 µL of reaction buffer (320 mM

glycine, 320 mM hydrazine, 2.4 mM NAD^+ and 2 U/mL of lactate dehydrogenase (LDH). After 30 minutes of incubation at room temperature, the lactate-dependent generation of NADH was measured at 340 nm using the Infinite 200 PRO multimode reader (Tecan). Lactate levels were normalized by total protein levels, quantified using Pierce BCA Protein Assay Kit (Thermo Scientific).

Glucose and glutamine incorporation into lipids

Neurons were grown on glass coverslips for 48 hours in a medium containing 0.8 μCi/ml ^{14}C-U-glucose (Perkin-Elmer) or 2 μCi/ml L-3-4-^{3}H(N)-glutamine (Perkin Elmer). Lipid isolation was performed as described previously by Folch et al. (Folch et al, 1957). See supplementary information

ATP measurement

ATP levels were measured using the ATPlite Luminescence Assay System (Perkin-Elmer) on the Infinite 200 PRO multimode reader (TECAN) following the manufacteurer's instructions. ATP levels were normalized by total protein levels, quantified using Pierce BCA Protein Assay Kit (Thermo Scientific).

Statistical analysis

Statistical analysis involved two-tailed Student's t-tests. For any multiple comparisons within data sets, we used a one-way ANOVA followed by Tukey's post-hoc test. All data are presented as the mean ± s.e.m. of at least three independent experiments (n). A p value less than 0.05 was considered statistically significant.

Author contributions

MS-M designed and performed most of the experiments and analyzed data; SC-D, MR-P, CM-S designed and performed experiments and analyzed data; AM-R and IH performed experiments and analyzed data; JA performed HIF-1α gene inactivation in vivo and had critical input into the manuscript preparation; MR and OMM-E analyzed data and had critical input into the manuscript preparation; FXS conceived, designed and performed experiments, analyzed data, and wrote the manuscript.

Conflict of interest

The authors declare that they have no conflict of interest.

Acknowledgments

This work was supported by research grants from the Spanish Ministerio de Economía y Competitividad/FEDER funds (SAF2011-30283 and SAF2014-59872-P to FXS; SAF2016-76815-R to JA; BFU2015-68135-P to OMM-E) and Fundación Ramón Areces (to OMM-S). MS-M is the recipient of a predoctoral fellowship from Fundación Tatiana Pérez de Guzmán el Bueno.

References

Agostini M, Romeo F, Inoue S, Niklison-Chirou MV, Elia AJ, Dinsdale D, Morone N, Knight RA, Mak TW, Melino G (2016) Metabolic reprogramming during neuronal differentiation. *Cell Death Differ* **23:** 1502-1514

Ahn S, Olive M, Aggarwal S, Krylov D, Ginty DD, Vinson C (1998) A Dominant-Negative Inhibitor of CREB Reveals that It Is a General Mediator of Stimulus-Dependent Transcription of c-fos. *Molecular and Cellular Biology* **18:** 967-977

Altarejos JY, Montminy M (2011) CREB and the CRTC co-activators: sensors for hormonal and metabolic signals. *Nature reviews Molecular cell biology* **12:** 141-151

Ashrafi G, Wu Z, Farrell RJ, Ryan TA (2017) GLUT4 Mobilization Supports Energetic Demands of Active Synapses. *Neuron* **93:** 606-615.e603

Bading H (2013) Nuclear calcium signalling in the regulation of brain function. *Nat Rev Neurosci* **14:** 593-608

Bas-Orth C, Tan Y-W, Lau D, Bading H (2017) Synaptic Activity Drives a Genomic Program That Promotes a Neuronal Warburg Effect. *Journal of Biological Chemistry* **292:** 5183-5194

Bélanger M, Allaman I, Magistretti Pierre J (2011) Brain Energy Metabolism: Focus on Astrocyte-Neuron Metabolic Cooperation. *Cell Metabolism* **14:** 724-738

Burr Stephen P, Costa Ana SH, Grice Guinevere L, Timms Richard T, Lobb Ian T, Freisinger P, Dodd Roger B, Dougan G, Lehner Paul J, Frezza C, Nathan James A (2016) Mitochondrial Protein Lipoylation and the 2-Oxoglutarate Dehydrogenase Complex Controls HIF1α Stability in Aerobic Conditions. *Cell Metabolism* **24:** 740-752

Denko NC (2008) Hypoxia, HIF1 and glucose metabolism in the solid tumour. *Nat Rev Cancer* **8:** 705-713

Díaz-García CM, Mongeon R, Lahmann C, Koveal D, Zucker H, Yellen G (2017) Neuronal Stimulation Triggers Neuronal Glycolysis and Not Lactate Uptake. *Cell Metabolism* **26:** 361-374.e364

Dienel GA (2017) Lack of appropriate stoichiometry: Strong evidence against an energetically important astrocyte-neuron lactate shuttle in brain. *Journal of neuroscience research*

Divakaruni AS, Wallace M, Buren C, Martyniuk K, Andreyev AY, Li E, Fields JA, Cordes T, Reynolds IJ, Bloodgood BL, Raymond LA, Metallo CM, Murphy AN (2017) Inhibition of the mitochondrial pyruvate carrier protects from excitotoxic neuronal death. *The Journal of Cell Biology* **216:** 1091-1105

Dotti C, Sullivan C, Banker G (1988) The establishment of polarity by hippocampal neurons in culture. *The Journal of Neuroscience* **8:** 1454-1468

Faherty CJ, Kerley D, Smeyne RJ (2003) A Golgi-Cox morphological analysis of neuronal changes induced by environmental enrichment. *Developmental Brain Research* **141:** 55-61

Ferreira JM, Burnett AL, Rameau GA (2011) Activity-Dependent Regulation of Surface Glucose Transporter-3. *The Journal of Neuroscience* **31:** 1991-1999

Folch J, Lees M, Sloane Stanley GH (1957) A simple method for the isolation and purification of total lipides from animal tissues. *J Biol Chem* **226:** 497-509

Frew IJ, Hammond VE, Dickins RA, Quinn JMW, Walkley CR, Sims NA, Schnall R, Della NG, Holloway AJ, Digby MR, Janes PW, Tarlinton DM, Purton LE, Gillespie MT, Bowtell DDL (2003) Generation and Analysis of Siah2 Mutant Mice. *Molecular and Cellular Biology* **23:** 9150-9161

Fünfschilling U, Jockusch WJ, Sivakumar N, Möbius W, Corthals K, Li S, Quintes S, Kim Y, Schaap IAT, Rhee J-S, Nave K-A, Saher G (2012) Critical Time Window of Neuronal Cholesterol Synthesis during Neurite Outgrowth. *The Journal of Neuroscience* **32:** 7632-7645

Goldberg JL (2003) How does an axon grow? *Genes & Development* **17:** 941-958

Goldberg JL, Espinosa JS, Xu Y, Davidson N, Kovacs GTA, Barres BA (2002) Retinal Ganglion Cells Do Not Extend Axons by Default. *Neuron* **33:** 689-702

Goyal Manu S, Hawrylycz M, Miller Jeremy A, Snyder Abraham Z, Raichle Marcus E (2014) Aerobic Glycolysis in the Human Brain Is Associated with Development and Neotenous Gene Expression. *Cell Metabolism* **19:** 49-57

Greer PL, Greenberg ME (2008) From Synapse to Nucleus: Calcium-Dependent Gene Transcription in the Control of Synapse Development and Function. *Neuron* **59:** 846-860

Groc L, Petanjek Z, Gustafsson B, Ben-Ari Y, Hanse E, Khazipov R (2002) In vivo blockade of neural activity alters dendritic development of neonatal CA1 pyramidal cells. *European Journal of Neuroscience* **16:** 1931-1938

Habelhah H, Laine A, Erdjument-Bromage H, Tempst P, Gershwin ME, Bowtell DDL, Ronai Ze (2004) Regulation of 2-Oxoglutarate (α-Ketoglutarate) Dehydrogenase Stability by the RING Finger Ubiquitin Ligase Siah. *Journal of Biological Chemistry* **279:** 53782-53788

Hardingham GE, Arnold FJL, Bading H (2001) Nuclear calcium signaling controls CREB-mediated gene expression triggered by synaptic activity. *Nat Neurosci* **4:** 261-267

Harris Julia J, Jolivet R, Attwell D (2012) Synaptic Energy Use and Supply. *Neuron* **75:** 762-777

Hausott B, Vallant N, Auer M, Yang L, Dai F, Brand-Saberi B, Klimaschewski L (2009) Sprouty2 down-regulation promotes axon growth by adult sensory neurons. *Molecular and Cellular Neuroscience* **42:** 328-340

Hausott B, Vallant N, Schlick B, Auer M, Nimmervoll B, Obermair GJ, Schwarzer C, Dai F, Brand-Saberi B, Klimaschewski L (2012) Sprouty2 and -4 regulate axon outgrowth by hippocampal neurons. *Hippocampus* **22:** 434-441

Helton R, Cui J, Scheel JR, Ellison JA, Ames C, Gibson C, Blouw B, Ouyang L, Dragatsis I, Zeitlin S, Johnson RS, Lipton SA, Barlow C (2005) Brain-Specific Knock-Out of Hypoxia-Inducible Factor-1α Reduces Rather Than Increases Hypoxic-Ischemic Damage. *The Journal of Neuroscience* **25:** 4099-4107

Hicks KC, Patel TB (2016) Sprouty2 Protein Regulates Hypoxia-inducible Factor-α (HIFα) Protein Levels and Transcription of HIFα-responsive Genes. *Journal of Biological Chemistry* **291:** 16787-16801

Intlekofer AM, Wang B, Liu H, Shah H, Carmona-Fontaine C, Rustenburg AS, Salah S, Gunner MR, Chodera JD, Cross JR, Thompson CB (2017) L-2-Hydroxyglutarate production arises from noncanonical enzyme function at acidic pH. *Nat Chem Biol* **13:** 494-500

Ivan M, Kondo K, Yang H, Kim W, Valiando J, Ohh M, Salic A, Asara JM, Lane WS, Kaelin Jr. WG (2001) HIFα Targeted for VHL-Mediated Destruction by Proline Hydroxylation: Implications for O₂ Sensing. *Science* **292:** 464-468

Iyer NV, Kotch LE, Agani F, Leung SW, Laughner E, Wenger RH, Gassmann M, Gearhart JD, Lawler AM, Yu AY, Semenza GL (1998) Cellular and developmental control of O2 homeostasis by hypoxia-inducible factor 1α. *Genes & Development* **12:** 149-162

Jaakkola P, Mole DR, Tian Y-M, Wilson MI, Gielbert J, Gaskell SJ, Kriegsheim Av, Hebestreit HF, Mukherji M, Schofield CJ, Maxwell PH, Pugh CW, Ratcliffe PJ (2001) Targeting of HIF-α to the von Hippel-Lindau Ubiquitylation Complex by O₂-Regulated Prolyl Hydroxylation. *Science* **292:** 468-472

Jang S, Nelson Jessica C, Bend Eric G, Rodríguez-Laureano L, Tueros Felipe G, Cartagenova L, Underwood K, Jorgensen Erik M, Colón-Ramos Daniel A Glycolytic Enzymes Localize to Synapses under Energy Stress to Support Synaptic Function. *Neuron* **90:** 278-291

Kaufmann WE, Moser HW (2000) Dendritic anomalies in disorders associated with mental retardation. *Cerebral cortex* **10:** 981-991

Konur S, Ghosh A Calcium Signaling and the Control of Dendritic Development. *Neuron* **46:** 401-405

Li C, Park S, Zhang X, Dai W, Xu D (2017) Mutual regulation between Polo-like kinase 3 and SIAH2 E3 ubiquitin ligase defines a regulatory network that fine-tunes the cellular response to hypoxia and nickel. *Journal of Biological Chemistry* **292:** 11431-11444

Li Y-X, Zhang Y, Lester HA, Schuman EM, Davidson N (1998) Enhancement of Neurotransmitter Release Induced by Brain-Derived Neurotrophic Factor in Cultured Hippocampal Neurons. *The Journal of Neuroscience* **18:** 10231-10240

Longair MH, Baker DA, Armstrong JD (2011) Simple Neurite Tracer: open source software for reconstruction, visualization and analysis of neuronal processes. *Bioinformatics* **27:** 2453-2454

Lonze BE, Ginty DD (2002) Function and Regulation of CREB Family Transcription Factors in the Nervous System. *Neuron* **35:** 605-623

Lonze BE, Riccio A, Cohen S, Ginty DD (2002) Apoptosis, Axonal Growth Defects, and Degeneration of Peripheral Neurons in Mice Lacking CREB. *Neuron* **34:** 371-385

Lu H, Forbes RA, Verma A (2002) Hypoxia-inducible Factor 1 Activation by Aerobic Glycolysis Implicates the Warburg Effect in Carcinogenesis. *Journal of Biological Chemistry* **277:** 23111-23115

Lundgaard I, Li B, Xie L, Kang H, Sanggaard S, Haswell JDR, Sun W, Goldman S, Blekot S, Nielsen M, Takano T, Deane R, Nedergaard M (2015) Direct neuronal glucose uptake heralds activity-dependent increases in cerebral metabolism. *Nature Communications* **6:** 6807

Magistretti Pierre J, Allaman I (2015) A Cellular Perspective on Brain Energy Metabolism and Functional Imaging. *Neuron* **86:** 883-901

Martorell-Riera A, Segarra-Mondejar M, Reina M, Martínez-Estrada OM, Soriano FX (2015) Mitochondrial fragmentation in excitotoxicity requires ROCK activation. *Cell Cycle* **14:** 1365-1369

Marvaldi L, Thongrong S, Kozłowska A, Irschick R, Pritz CO, Bäumer B, Ronchi G, Geuna S, Hausott B, Klimaschewski L (2015) Enhanced axon outgrowth and improved long-distance axon regeneration in sprouty2 deficient mice. *Developmental Neurobiology* **75:** 217-231

Maxwell PH, Wiesener MS, Chang G-W, Clifford SC, Vaux EC, Cockman ME, Wykoff CC, Pugh CW, Maher ER, Ratcliffe PJ (1999) The tumour suppressor protein VHL targets hypoxia-inducible factors for oxygen-dependent proteolysis. *Nature* **399:** 271-275

Molina CA, Foulkes NS, Lalli E, Sassone-Corsi P (1993) Inducibility and negative autoregulation of CREM: an alternative promoter directs the expression of ICER, an early response repressor. *Cell* **75:** 875-886

Nadtochiy SM, Schafer X, Fu D, Nehrke K, Munger J, Brookes PS (2016) Acidic pH Is a Metabolic Switch for 2-Hydroxyglutarate Generation and Signaling. *Journal of Biological Chemistry* **291:** 20188-20197

Nakayama K, Frew IJ, Hagensen M, Skals M, Habelhah H, Bhoumik A, Kadoya T, Erdjument-Bromage H, Tempst P, Frappell PB, Bowtell DD, Ronai Ze (2004) Siah2 Regulates Stability of Prolyl-Hydroxylases, Controls HIF1α Abundance, and Modulates Physiological Responses to Hypoxia. *Cell* **117:** 941-952

Ohira K, Kumanogoh H, Sahara Y, Homma KJ, Hirai H, Nakamura S, Hayashi M (2005) A Truncated Tropo-Myosine-Related Kinase B Receptor, T1, Regulates Glial Cell Morphology via Rho GDP Dissociation Inhibitor 1. *The Journal of Neuroscience* **25:** 1343-1353

Papadia S, Soriano FX, Leveille F, Martel MA, Dakin KA, Hansen HH, Kaindl A, Sifringer M, Fowler J, Stefovska V, McKenzie G, Craigon M, Corriveau R, Ghazal P, Horsburgh K, Yankner BA, Wyllie DJ, Ikonomidou C, Hardingham GE (2008) Synaptic NMDA receptor activity boosts intrinsic antioxidant defenses. *Nat Neurosci* **11:** 476-487

Park H, Poo M-m (2013) Neurotrophin regulation of neural circuit development and function. *Nat Rev Neurosci* **14:** 7-23

Pascual JM, Wang D, Hinton V, et al. (2007) Brain glucose supply and the syndrome of infantile neuroglycopenia. *Archives of Neurology* **64:** 507-513

Patel AB, Lai JCK, Chowdhury GMI, Hyder F, Rothman DL, Shulman RG, Behar KL (2014) Direct evidence for activity-dependent glucose phosphorylation in neurons with implications for the astrocyte-to-neuron lactate shuttle. *Proceedings of the National Academy of Sciences* **111:** 5385-5390

Pellerin L, Magistretti PJ (1994) Glutamate uptake into astrocytes stimulates aerobic glycolysis: a mechanism coupling neuronal activity to glucose utilization. *Proc Natl Acad Sci U S A* **91:** 10625-10629

Pellerin L, Magistretti PJ (2012) Sweet Sixteen for ANLS. *Journal of Cerebral Blood Flow & Metabolism* **32:** 1152-1166

Pfenninger KH (2009) Plasma membrane expansion: a neuron's Herculean task. *Nat Rev Neurosci* **10:** 251-261

Pietrocola F, Galluzzi L, Bravo-San Pedro JM, Madeo F, Kroemer G (2015) Acetyl coenzyme A: a central metabolite and second messenger. *Cell Metab* **21:** 805-821

Puram SV, Bonni A (2013) Cell-intrinsic drivers of dendrite morphogenesis. *Development* **140:** 4657-4671

Qi J, Nakayama K, Gaitonde S, Goydos JS, Krajewski S, Eroshkin A, Bar-Sagi D, Bowtell D, Ronai Ze (2008) The ubiquitin ligase Siah2 regulates tumorigenesis and metastasis by HIF-dependent and -independent pathways. *Proceedings of the National Academy of Sciences* **105:** 16713-16718

Rajakumar A, Thamotharan S, Raychaudhuri N, Menon RK, Devaskar SU (2004) Trans-activators Regulating Neuronal Glucose Transporter Isoform-3 Gene Expression in Mammalian Neurons. *Journal of Biological Chemistry* **279:** 26768-26779

Rajan I, Cline HT (1998) Glutamate Receptor Activity Is Required for Normal Development of Tectal Cell Dendrites In Vivo. *The Journal of Neuroscience* **18:** 7836-7846

Rangaraju V, Calloway N, Ryan Timothy A (2014) Activity-Driven Local ATP Synthesis Is Required for Synaptic Function. *Cell* **156:** 825-835

Redmond L, Kashani AH, Ghosh A (2002) Calcium Regulation of Dendritic Growth via CaM Kinase IV and CREB-Mediated Transcription. *Neuron* **34:** 999-1010

Rose CR, Blum R, Pichler B, Lepier A, Kafitz KW, Konnerth A (2003) Truncated TrkB-T1 mediates neurotrophin-evoked calcium signalling in glia cells. *Nature* **426:** 74-78

Ryan HE, Lo J, Johnson RS (1998) HIF-1α is required for solid tumor formation and embryonic vascularization. *The EMBO Journal* **17:** 3005-3015

Schneider CA, Rasband WS, Eliceiri KW (2012) NIH Image to ImageJ: 25 years of image analysis. *Nat Meth* **9:** 671-675

Schoors S, De Bock K, Cantelmo Anna R, Georgiadou M, Ghesquière B, Cauwenberghs S, Kuchnio A, Wong Brian W, Quaegebeur A, Goveia J, Bifari F, Wang X, Blanco R, Tembuyser B, Cornelissen I, Bouché A, Vinckier S, Diaz-Moralli S, Gerhardt H, Telang S, Cascante M, Chesney J, Dewerchin M, Carmeliet P (2014) Partial and Transient Reduction of Glycolysis by PFKFB3 Blockade Reduces Pathological Angiogenesis. *Cell Metabolism* **19:** 37-48

Semenza GL (2017) A compendium of proteins that interact with HIF-1α. *Experimental Cell Research* **356:** 128-135

Semenza GL, Roth PH, Fang HM, Wang GL (1994) Transcriptional regulation of genes encoding glycolytic enzymes by hypoxia-inducible factor 1. *Journal of Biological Chemistry* **269:** 23757-23763

Silbereis John C, Pochareddy S, Zhu Y, Li M, Sestan N (2016) The Cellular and Molecular Landscapes of the Developing Human Central Nervous System. *Neuron* **89:** 248-268

Silver I, Erecinska M (1994) Extracellular glucose concentration in mammalian brain: continuous monitoring of changes during increased neuronal activity and upon limitation in oxygen supply in normo-, hypo-, and hyperglycemic animals. *The Journal of Neuroscience* **14:** 5068-5076

Soriano FX, Léveillé F, Papadia S, Higgins LG, Varley J, Baxter P, Hayes JD, Hardingham GE (2008) Induction of sulfiredoxin expression and reduction of peroxiredoxin hyperoxidation by the neuroprotective Nrf2 activator 3H-1,2-dithiole-3-thione. *Journal of Neurochemistry* **107:** 533-543

Soro-Arnaiz I, Li Qilong Oscar Y, Torres-Capelli M, Meléndez-Rodríguez F, Veiga S, Veys K, Sebastian D, Elorza A, Tello D, Hernansanz-Agustín P, Cogliati S, Moreno-Navarrete Jose M, Balsa E, Fuertes E, Romanos E, Martínez-Ruiz A, Enriquez Jose A, Fernandez-Real Jose M, Zorzano A, De Bock K, Aragonés J (2016) Role of Mitochondrial Complex IV in Age-Dependent Obesity. *Cell Reports* **16:** 2991-3002

Sun Ramon C, Denko Nicholas C (2014) Hypoxic Regulation of Glutamine Metabolism through HIF1 and SIAH2 Supports Lipid Synthesis that Is Necessary for Tumor Growth. *Cell Metabolism* **19:** 285-292

TeSlaa T, Teitell MA (2014) Chapter Five - Techniques to Monitor Glycolysis. In *Methods in Enzymology*, Galluzzi L, Kroemer G (eds), Vol. 542, pp 91-114. Academic Press

Tomita S, Ueno M, Sakamoto M, Kitahama Y, Ueki M, Maekawa N, Sakamoto H, Gassmann M, Kageyama R, Ueda N, Gonzalez FJ, Takahama Y (2003) Defective Brain Development in Mice Lacking the Hif-1α Gene in Neural Cells. *Molecular and Cellular Biology* **23:** 6739-6749

Vaishnavi SN, Vlassenko AG, Rundle MM, Snyder AZ, Mintun MA, Raichle ME (2010) Regional aerobic glycolysis in the human brain. *Proceedings of the National Academy of Sciences* **107:** 17757-17762

Vander Heiden MG, Cantley LC, Thompson CB (2009) Understanding the Warburg Effect: The Metabolic Requirements of Cell Proliferation. *Science* **324:** 1029-1033

Wong ROL, Ghosh A (2002) Activity-dependent regulation of dendritic growth and patterning. *Nat Rev Neurosci* **3:** 803-812

Xu D, Yao Y, Lu L, Costa M, Dai W (2010) Plk3 Functions as an Essential Component of the Hypoxia Regulatory Pathway by Direct Phosphorylation of HIF-1α. *Journal of Biological Chemistry* **285:** 38944-38950

Zala D, Hinckelmann M-V, Yu H, Lyra da Cunha Marcel M, Liot G, Cordelières Fabrice P, Marco S, Saudou F (2013) Vesicular Glycolysis Provides On-Board Energy for Fast Axonal Transport. *Cell* **152:** 479-491

Zhang W, Guo C, Jiang K, Ying M, Hu X (2017) Quantification of lactate from various metabolic pathways and quantification issues of lactate isotopologues and isotopmers. *Scientific reports* **7:** 8489

Figure legends

Figure 1. Glucose uptake is necessary for activity-dependent neurite outgrowth. Untrunsduced (A) or AAV-shGPI or AAV-sh-sc (control) (B) neurons were incubated with ^{14}C-U-glucose were stimulated with bicuculline plus 4-AP (labeled Bic in this and subsequent figures) for 48 hours or left unstimulated (CT). Cellular lipids were extracted and radioactive counts measured (n= 4-7 independent experiments). Values represent mean ± s.e.m. *p<0.05, two-tailed Student's t-test (A) and ANOVA one-way ANOVA followed by Tukey's post-hoc test (B). C) Cortical neurons were stimulated for 24 hours with Bic+4-AP in the presence of glucose (n= 8 independent experiments). After 24 hours total acetyl-CoA levels were assayed. Values represent mean ± s.e.m. *p<0.05, two-tailed Student's t-test. D) Determination of cytosolic acetyl-CoA levels after 24 hours of Bic+4-AP stimulation in the presence of glucose (n= 4 independent experiments). Values represent mean ± s.e.m. *p<0.05, two-tailed Student's t-test. E) Acetyl-CoA levels in cortical neurons stimulated for 24 hours with Bic+4-AP in the presence of 25 mM of the non-metabolizable glucose analog 2-DG (n= 4 independent experiments). F) ^{14}C-U-glucose incorporation into lipids in neurons transduced with AAV expressing shRNA-sc or targeting ACLY (sh-ACLY) after 48 hours stimulation with Bic+4-AP. (n= 7 independent experiments). Values represent mean ± s.e.m. *p<0.05, one-way ANOVA

followed by Tukey post-hoc test. G and H) Neurite length and representative tracings of the neuritic tree of control and Bic+4-AP stimulated neurons (for 48 hours) after transfection with non-targeting (siC) or Glut3-targeting (siGlut3) siRNAs (n= 45-49 neurons from 9 independent experiments). Scale bar, 500 μm. Values represent mean ± s.e.m. *p<0.05, one-way ANOVA followed by Tukey's post-hoc test.

Figure 2. Synaptic activity stimulates neuronal glucose uptake and metabolism at the transcriptional level. A) 2-NBDG uptake over 15 minutes in control or Bic+4-AP stimulated (for 24 h) neurons after washing and medium replacement (n= 4 independent experiments). Values represent mean ± s.e.m. *p<0.05, two-tailed Student's t-test. B) Neurons treated or not with cycloheximide (10 μM) were stimulated with Bic+4-AP (for 24 h) before measuring the amount of lactate released into the medium (n= 4-7 independent experiments). Values represent mean ± s.e.m. *p<0.05, two-tailed Student's t-test. C) ATP levels in unstimulated neurons that were treated with CCCP (3 nM) following the indicated chronogram. + or – glucose indicates whether the fresh medium added after the wash step contained glucose or not. (n= 3-6 independent experiments). Values represent mean ± s.e.m. *p<0.05, two-tailed Student's t-test. D) Cortical neurons were stimulated with Bic+4-AP for 4 or 24 hours and mRNA expression of the indicated genes was determined by real-time qPCR (n= 3-6 independent experiments). Values represent mean ± s.e.m. *p<0.05, two-tailed Student's t-test. E) Representative western blot and (F) densitometric analysis of protein samples from control and Bic+4-AP-stimulated (24 hours) (n= 3-4 independent experiments).

Figure 3. Activity-dependent induction of glycolysis genes depends on HIF-1a stabilization. A) Cortical neurons were stimulated with Bic+4-AP over various time points and the HIF-1α protein was analyzed by western blotting (n= 5 independent experiments). B) Densitomeric analysis of HIF-1α expression. Values represent mean ± s.e.m. *p<0.05, two-tailed Student's t-test. C) Luciferase-based HIF-1α activity in neurons expressing a control plasmid (globin) or a

dominant negative HIF-1α (HIF-DN) and stimulated with Bic+4-AP for 8 hours (n= 4 independent experiments). Values represent mean ± s.e.m. *p<0.05, one-way ANOVA followed by Tukey post-hoc test. D) Cortical neurons were transduced with AAV expressing HIF-DN or control (GFP), stimulated for 4 or 24 hours with Bic+4-AP and the mRNA expression of the indicated genes was analyzed by qPCR (n= 5 independent experiments). Values represent mean ± s.e.m. *p<0.05, one-way ANOVA followed by Tukey post-hoc test. E) Lactate released into the medium by neurons transduced with AAV expressing HIF-DN or control (GFP) after 24 hours stimulation with Bic+4-AP. (n= 3 independent experiments). Values represent mean ± s.e.m. *p<0.05, one-way ANOVA followed by Tukey post-hoc test. F) ^{14}C-U-glucose incorporation into lipids in neurons transduced with with AAV expressing HIF-DN or control (GFP) and stimulated for 48 hours with Bic+4-AP. (n= 4 independent experiments). Values represent mean ± s.e.m. *p<0.05, one-way ANOVA followed by Tukey post-hoc test.

Figure 4. HIF-1α is stabilized by Siah2 and LDH activity. A and B) PHD activity after Bic+4-AP stimulation was assayed measuring luciferase activity in neurons transfected with plasmids expressing luciferase fused to the ODD domain of HIF-1α. Non fused luciferase was used as control (n=4 independent experiments). Values represent mean ± s.e.m. *p<0.05, two-tailed Student's t-test. C) Cortical neurons were stimulated with Bic+4-AP for 4 or 24 hours and Siah2 mRNA expression was determined by real-time qPCR (n= 4 independent experiments). Values represent mean ± s.e.m. *p<0.05, two-tailed Student's t-test. D) Cortical neurons were stimulated with Bic+4-AP over various time points and the indicated proteins were analyzed by western blotting (n= 3-5 independent experiments). E) Densitometric analysis of Siah2 protein levels. Values represent mean ± s.e.m. *p<0.05, two-tailed Student's t-test. F) AAV sh-sc (control) or sh-Siah2 transduced neurons were stimulated with Bic+4-AP for 4 hours before analyzing the expression of the indicated proteins (n= 5 independent experiments).G) and H) Densitometric analysis of the indicated proteins. Values represent mean ± s.e.m. *p<0.05, one-way ANOVA followed by Tukey post-hoc test. I) Lactate released into the medium by neurons

transduced with AAV expressing shRNA-sc or targeting Siah2 (sh-Siah2) after 24 hours stimulation with Bic+4-AP. (n= 4 independent experiments). Values represent mean ± s.e.m. *p<0.05, one-way ANOVA followed by Tukey post-hoc test. J) ^{14}C-U-glucose incorporation into lipids in neurons transduced with AAV expressing shRNA-sc or targeting Siah2 (sh-Siah2) after 48 hours stimulation with Bic+4-AP. (n= 7 independent experiments). Values represent mean ± s.e.m. *p<0.05, one-way ANOVA followed by Tukey post-hoc test. K) Representative western blot and (L) densitometric analysis of neurons stimulated for 4 hours with Bic+4-AP in absence or presence of 40 mM oxamate (Oxam.). (n= 5 independent experiments). Values represent mean ± s.e.m. *p<0.05, one-way ANOVA followed by Tukey post-hoc test.

Figure 5. Glut3 and Siah2 expression is regulated by CREB. Cortical neurons transduced with AAV expressing GFP (control) or dominant negative A-CREB were stimulated with Bic+4-AP for 4 hours before analyzing the mRNA expression of (A) Glut3 and (B) Siah2 by qPCR (n= 5 independent experiments). Values represent mean ± s.e.m. *p<0.05, one-way ANOVA followed by Tukey's post-hoc test. C) Representative western blot and (D) and (E) densitometric analysis of the indicated proteins of neurons transduced with AAV expressing GFP or A-CREB and stimulated with Bic+4-AP for 4 hours (n= 3 independent experiments). Values represent mean ± s.e.m. *p<0.05, one-way ANOVA followed by Tukey post-hoc test. F) Luciferase-based HIF-1α activity in neurons expressing a control plasmid (globin) or a CREB inhibitor ICER and stimulated with Bic+4-AP for 8 hours (n= 5 independent experiments). Values represent mean ± s.e.m. *p<0.05, one-way ANOVA followed by Tukey's post-hoc test. G) CREB activator forskolin (FSK) was sufficient to induce Siah2 expression and stabilize HIF-1α. Representative western blot and densitometric analysis (H and I) of neurons treated with 10 μM forskolin for 4 hours (n= 3 independent experiments). *p<0.05, two-tailed Student's t-test. J) Luciferase-based HIF-1α activity in neurons treated with forskolin for 8 hours (n= 4 independent experiments). Values represent mean ± s.e.m. *p<0.05, two-tailed Student's t-test. K) CREB activation temporally precedes HIF-1α activation. Luciferase-based CREB and HIF-1α activity at

different time points after Bic+4-AP stimulation (n= 4 independent experiments). Values represent mean ± s.e.m. *p<0.05, two-tailed Student's t-test. L) Lactate released into the medium by neurons transduced with AAV expressing A-CREB or control (GFP) after 24 hours stimulation with Bic+4-AP. (n= 5 independent experiments). Values represent mean ± s.e.m. *p<0.05, one-way ANOVA followed by Tukey post-hoc test. M) ^{14}C-U-glucose incorporation into lipids in neurons transduced with with AAV expressing A-CREB or control (GFP) and stimulated for 48 hours with Bic+4-AP. (n= 5 independent experiments). Values represent mean ± s.e.m. *p<0.05, one-way ANOVA followed by Tukey post-hoc test.

Figure 6. Defective glycolysis impairs neurite growth. Analysis of neurite length of immature neurons transfected at DIV1 with GFP-expressing plasmids plus control plasmids (globin) or expressing HIF-1α (A), Siah2 (B) and analyzed 48 h after transfection and (C) representative tracings (n= 27-40 neurons from 6 independent experiments). Scale bar, 100 μm. Values represent mean ± s.e.m. *p<0.05, two-tailed Student's t-test. Analysis of neurite length and representative tracings of neurons transfected at DIV8 with GFP expressing plus plasmids control (globin) or expressing HIF-DN (D and E) or a non targeting siRNA (siCT) or a pool of 4 siRNAs targetins Siah2 (F and G) and stimulated the day after with Bic+4-AP for 48 hours (n= 27-36 neurons from 6 independent experiments). Scale bar, 500 μm. Values represent mean ± s.e.m. *p<0.05, one-way ANOVA followed by Tukey's post-hoc test. H) Sholl analysis and (I) representative tracings of Golgi-stained cortical neurons of 14 days old rats administered with 3PO (50 mg/kg) for 5 days. (n= 15-20 neurons from 4 mice per condition). Scale bar, 100 μm. Values represent mean ± s.e.m. *p<0.05, two-tailed Student's t-test. J) Immunohistochemical detection of HIF-1α in cortical sections from 10-day and 3-month old mice (n= 3 mice per condition). Scale bar, 50 μm. K) Immunfluorescence detection of HIF-1α, NeuN and GFAP in cortical sections from 10-day old mice (n= 3 mice per condition). Scale bar, 100 μm. L) Sholl analysis and (M) representative tracings of Golgi-stained cortical neurons of WT and early

postnatal deleted HIF-1α mice. (n= 16 neurons from 3 mice per condition). Scale bar, 100 μm. Values represent mean ± s.e.m. *p<0.05, two-tailed Student's t-test.

Figure 7. Model for synaptic activity inducing glucose metabolism to supply lipids for neurite growth. A) Synaptic activity induces glucose metabolism at transcriptional level: Synaptic activity (1) induces Ca^{2+} transients (2) that activate the transcription factor CREB (3). CREB upregulates Glut3 expression to increase glucose uptake by neurons. CREB also induces Siah2 expression that together with LDH activity promote the stabilization and activation of HIF-1α (4, 5), which in turn activates the expression of genes encoding the rate-limiting enzymes of glycolysis. B) Transcriptional changes induced by synaptic activity increase glucose uptake and enhance glycolytic flux. As a result, metabolites such as acetyl-CoA are generated and used for lipid synthesis necessary for membrane extension during neurite growth. Some graphics in the figure were obtained and modified from Smart Servier Medical Art (https://smart.servier.com/).

Figure 1

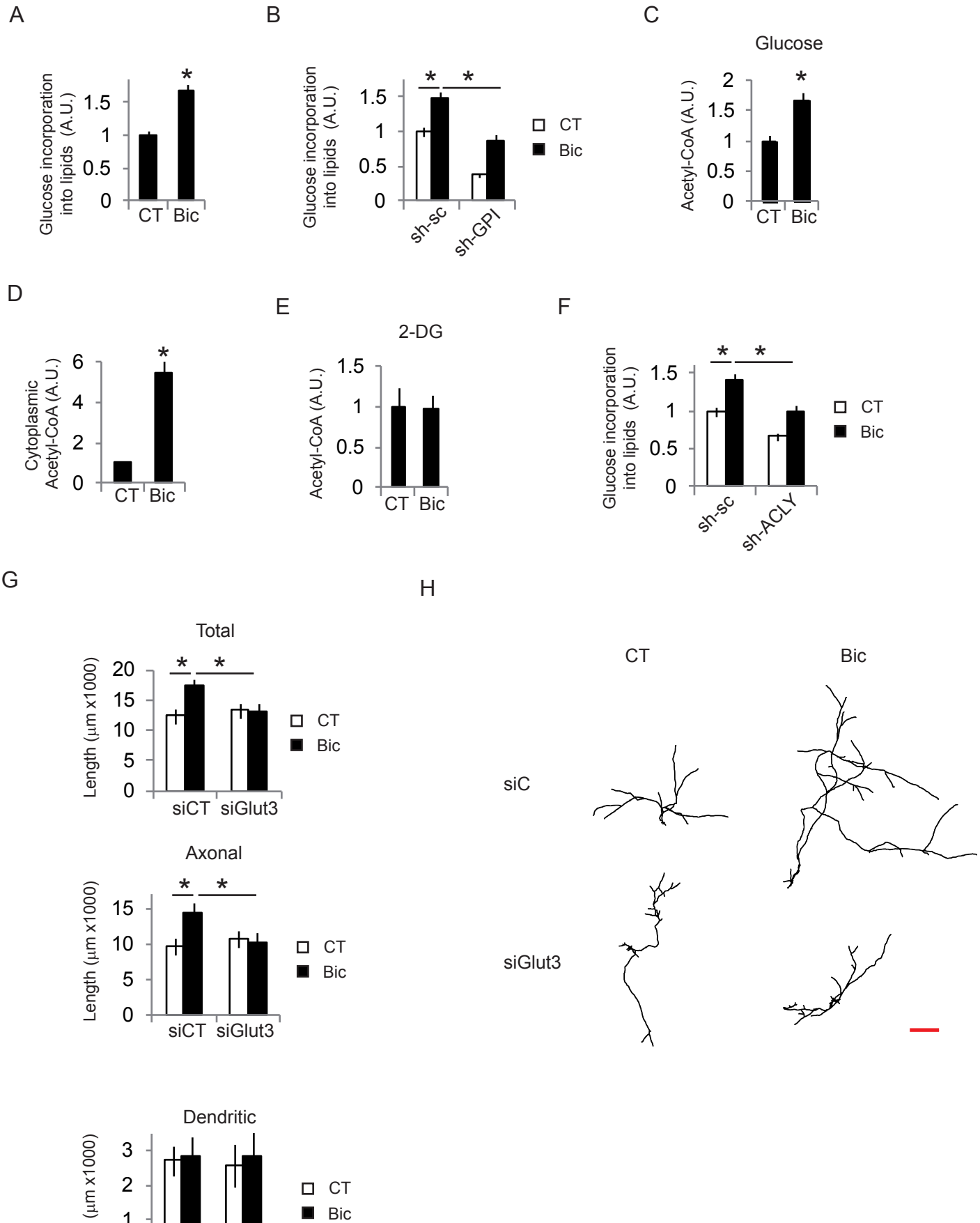
A
Glucose incorporation into lipids (A.U.)
CT
Bic
B
sh-sc
sh-GPI
C
Glucose
Acetyl-CoA (A.U.)
D
Cytoplasmic Acetyl-CoA (A.U.)
E
2-DG
F
sh-ACLY
G
Total
Axonal
Dendritic
Length (µm x1000)
siCT
siGlut3
H
siC
siGlut3

Figure 2

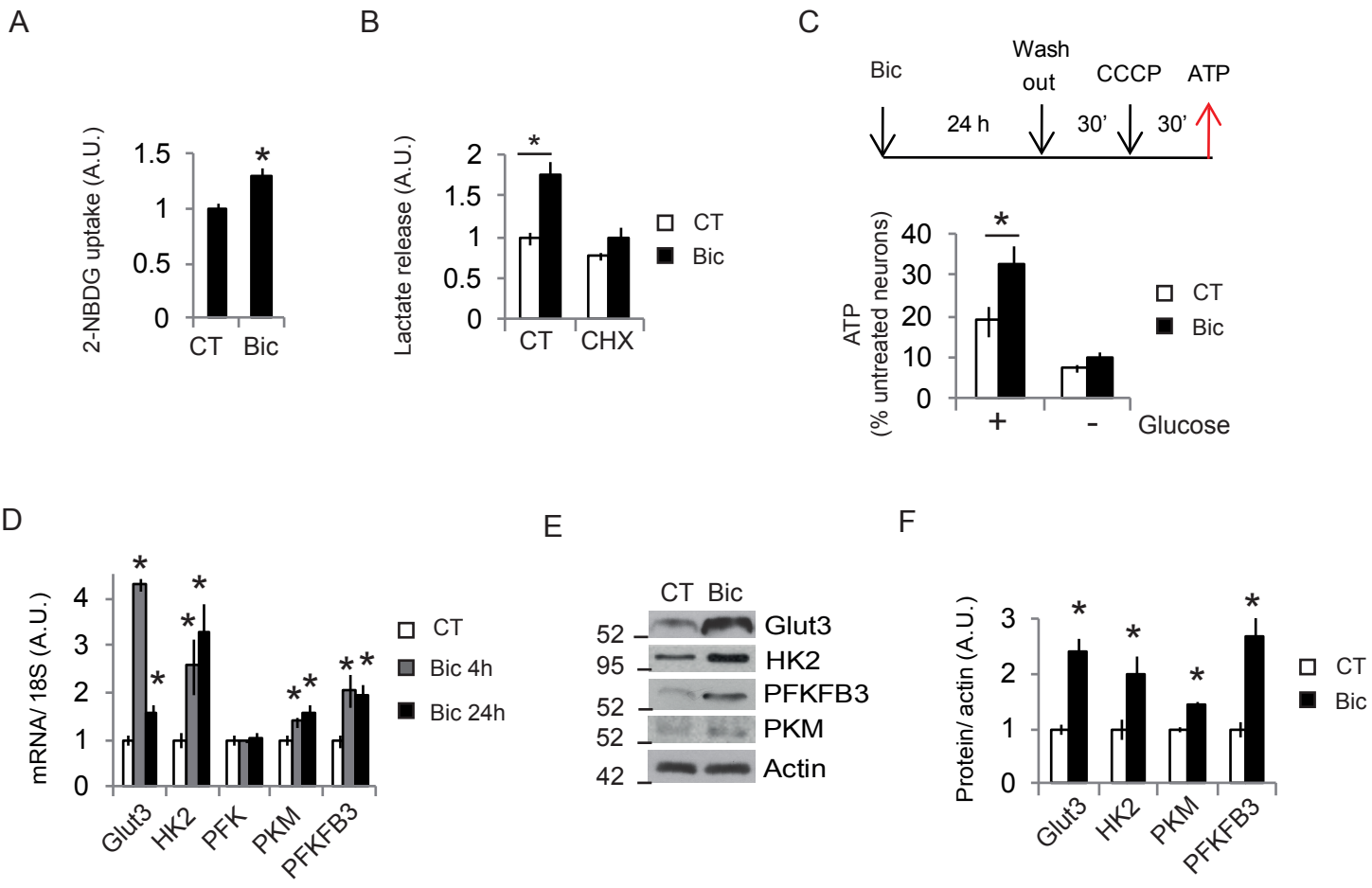
A
2-NBDG uptake (A.U.)
1.5
1
0.5
0
CT
Bic
B
Lactate release (A.U.)
2
1.5
1
0.5
0
CT
CHX
CT
Bic
C
Bic
Wash out
CCCP
ATP
24 h
30'
30'
ATP (% untreated neurons)
40
30
20
10
0
+
-
Glucose
CT
Bic
D
mRNA/ 18S (A.U.)
4
3
2
1
0
Glut3
HK2
PFK
PKM
PFKFB3
CT
Bic 4h
Bic 24h
E
CT Bic
52
95
52
52
42
Glut3
HK2
PFKFB3
PKM
Actin
F
Protein/ actin (A.U.)
3
2
1
0
Glut3
HK2
PKM
PFKFB3
CT
Bic

Figure 3

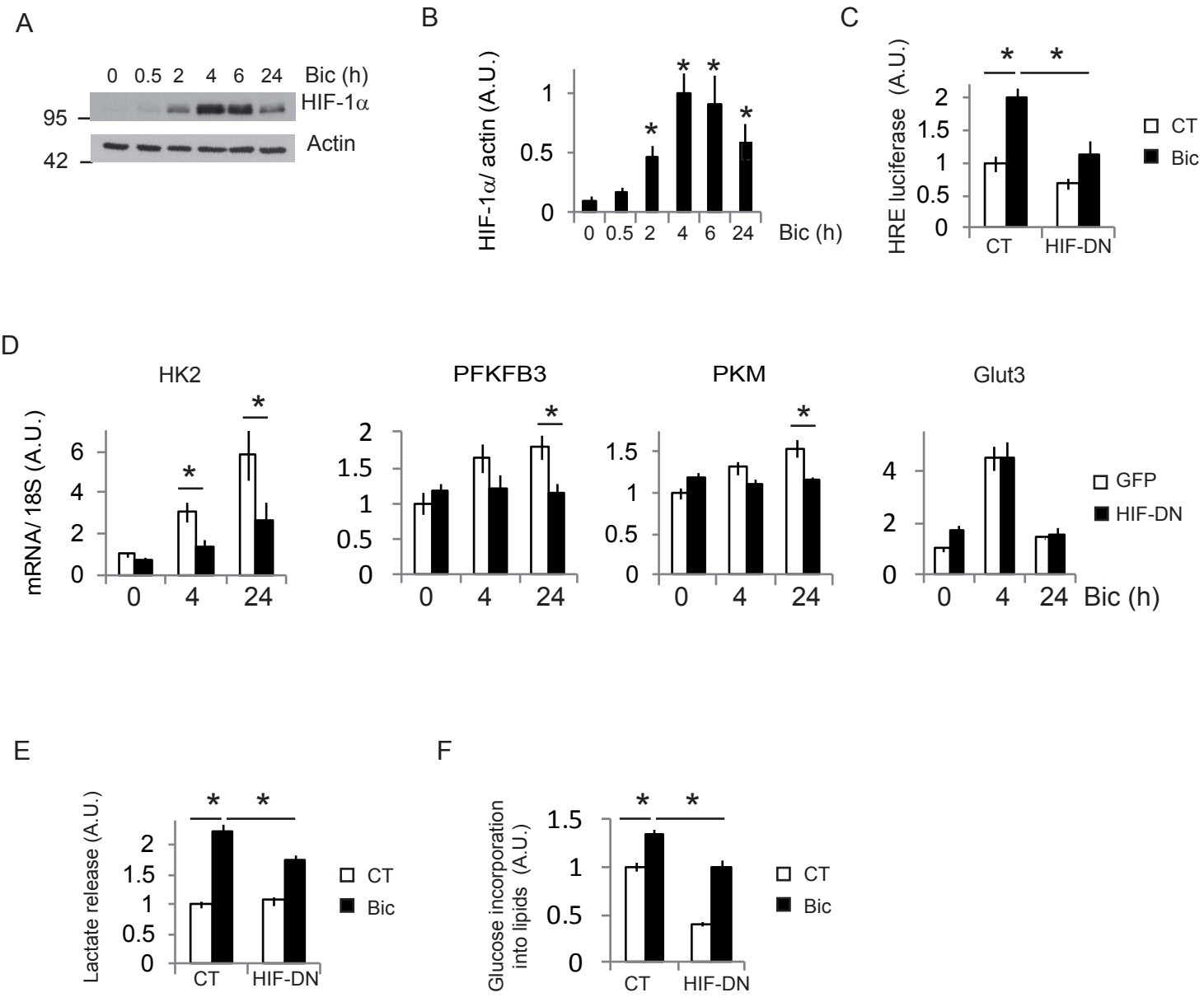
A
0 0.5 2 4 6 24 Bic (h)
95
HIF-1α
42
Actin
B
HIF-1α/ actin (A.U.)
0 0.5 2 4 6 24 Bic (h)
C
HRE luciferase (A.U.)
CT
HIF-DN
CT
Bic
D
HK2
PFKFB3
PKM
Glut3
mRNA/ 18S (A.U.)
0 4 24 Bic (h)
GFP
HIF-DN
E
Lactate release (A.U.)
CT
HIF-DN
CT
Bic
F
Glucose incorporation into lipids (A.U.)
CT
HIF-DN
CT
Bic

Figure 4

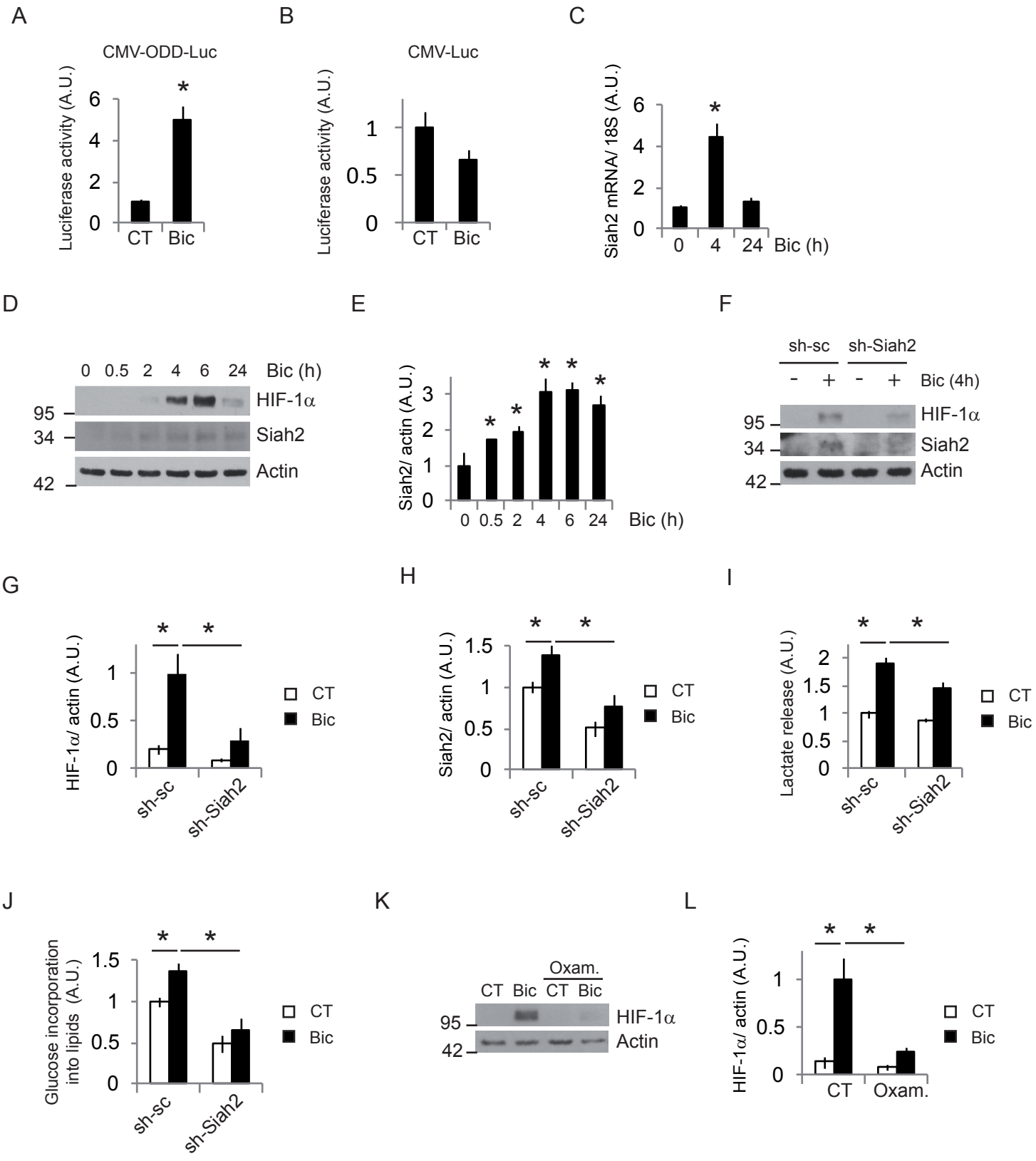
A
CMV-ODD-Luc
Luciferase activity (A.U.)
6
4
2
0
*
CT
Bic
B
CMV-Luc
Luciferase activity (A.U.)
1
0.5
0
CT
Bic
C
Siah2 mRNA/ 18S (A.U.)
6
4
2
0
*
0
4
24
Bic (h)
D
0 0.5 2 4 6 24 Bic (h)
95
34
42
HIF-1α
Siah2
Actin
E
Siah2/ actin (A.U.)
3
2
1
0
*
*
*
*
*
0 0.5 2 4 6 24
Bic (h)
F
sh-sc
sh-Siah2
- + - +
Bic (4h)
95
34
42
HIF-1α
Siah2
Actin
G
HIF-1α/ actin (A.U.)
1
0.5
0
*
*
sh-sc
sh-Siah2
CT
Bic
H
Siah2/ actin (A.U.)
1.5
1
0.5
0
*
*
sh-sc
sh-Siah2
CT
Bic
I
Lactate release (A.U.)
2
1.5
1
0.5
0
*
*
sh-sc
sh-Siah2
CT
Bic
J
Glucose incorporation into lipids (A.U.)
1.5
1
0.5
0
*
*
sh-sc
sh-Siah2
CT
Bic
K
Oxam.
CT Bic CT Bic
95
42
HIF-1α
Actin
L
HIF-1α/ actin (A.U.)
1
0.5
0
*
*
CT
Oxam.
CT
Bic

Figure 5

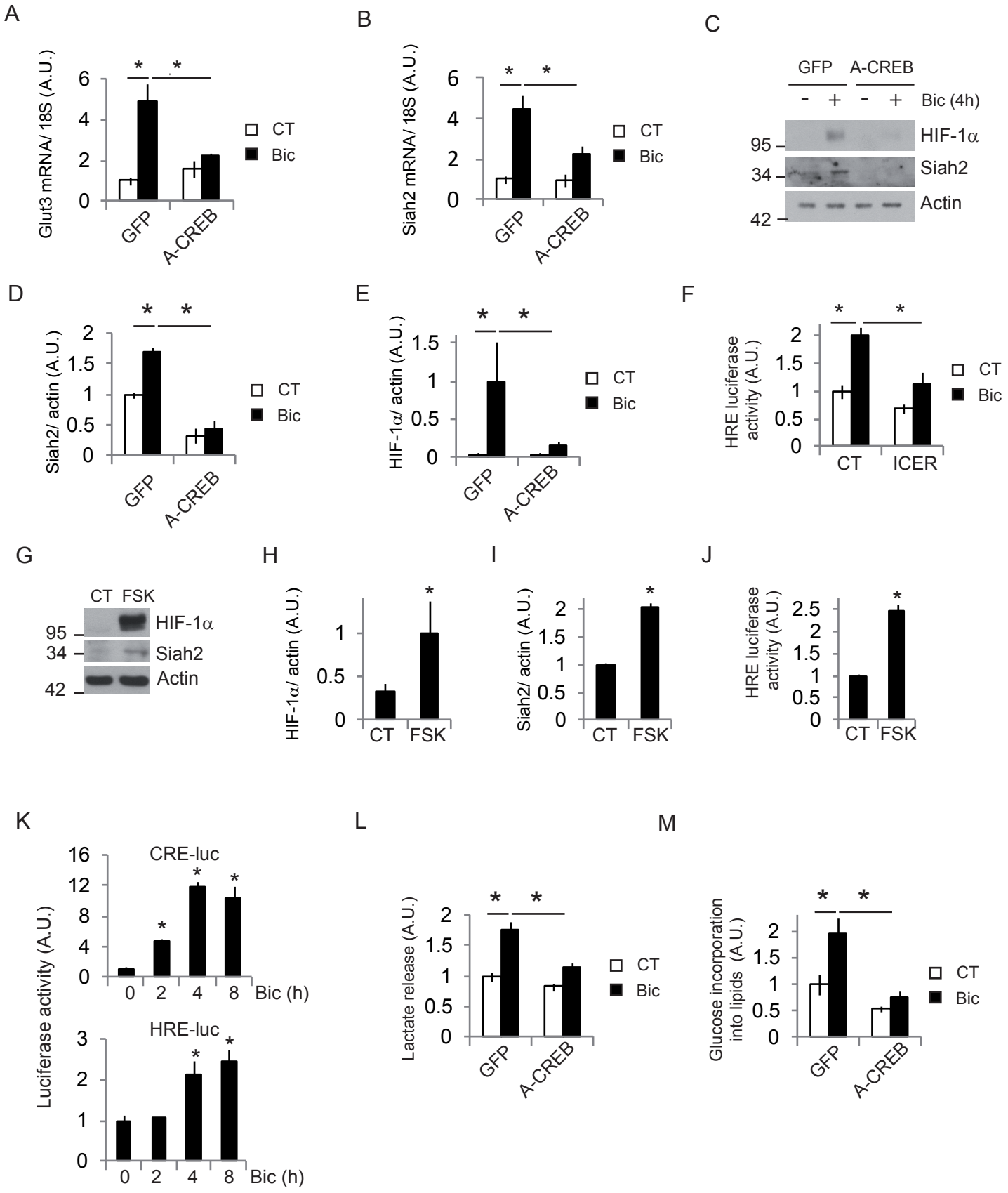
A
Glut3 mRNA/ 18S (A.U.)
CT
Bic
GFP
A-CREB
B
Siah2 mRNA/ 18S (A.U.)
C
GFP
A-CREB
Bic (4h)
HIF-1α
Siah2
Actin
95
34
42
D
Siah2/ actin (A.U.)
E
HIF-1α/ actin (A.U.)
F
HRE luciferase activity (A.U.)
CT
ICER
G
CT FSK
H
I
J
K
CRE-luc
HRE-luc
Luciferase activity (A.U.)
Bic (h)
L
Lactate release (A.U.)
M
Glucose incorporation into lipids (A.U.)

Figure 6

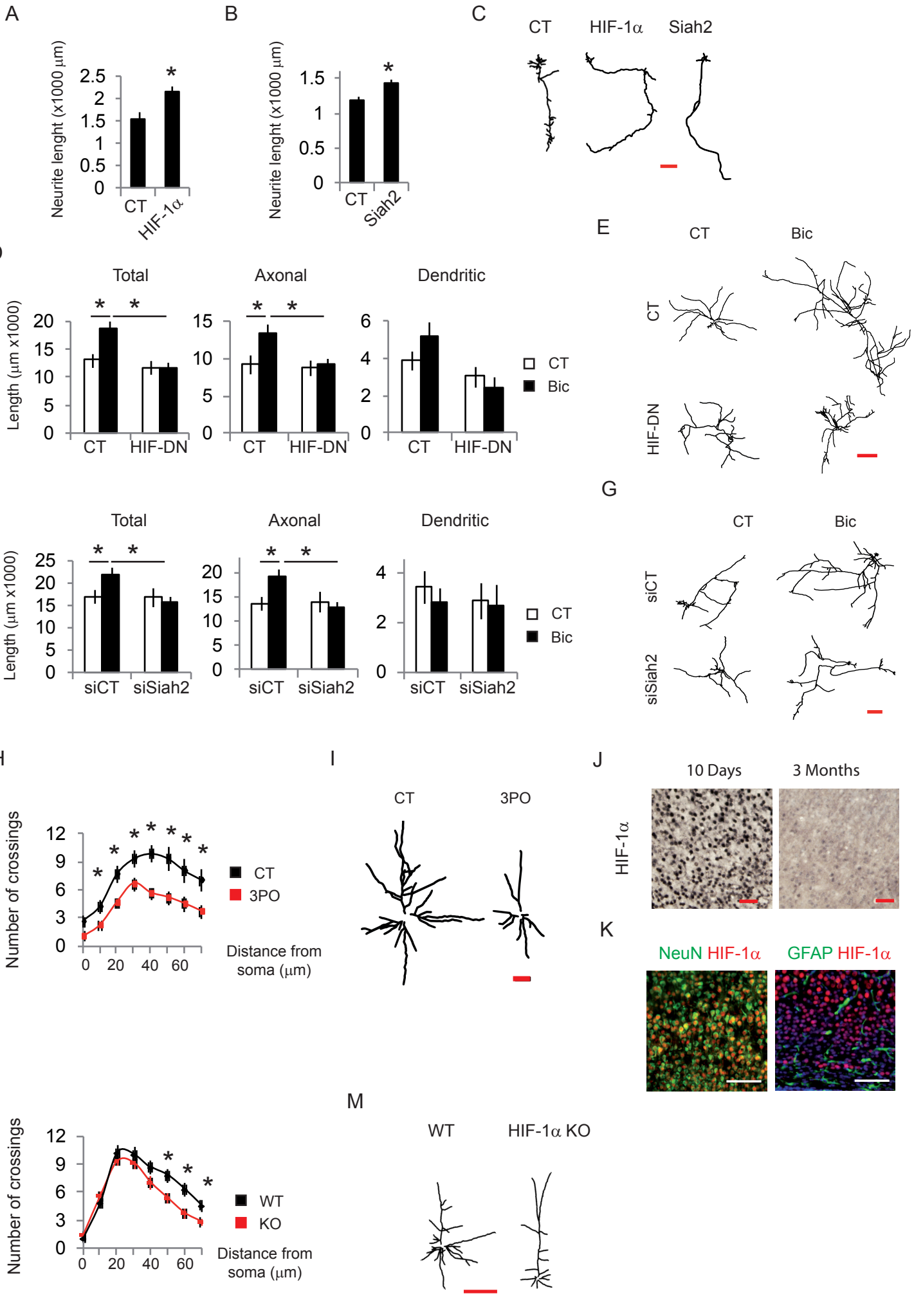
A
Neurite lenght (x1000 µm)
2.5
2
1.5
1
0.5
0
CT
HIF-1α
B
Neurite lenght (x1000 µm)
1.5
1
0.5
0
CT
Siah2
C
CT
HIF-1α
Siah2
D
Total
Axonal
Dendritic
Length (µm x1000)
20
15
10
5
0
6
4
2
CT
HIF-DN
CT
Bic
E
CT
Bic
CT
HIF-DN
F
Total
Axonal
Dendritic
Length (µm x1000)
25
20
15
10
5
0
4
2
siCT
siSiah2
CT
Bic
G
CT
Bic
siCT
siSiah2
H
Number of crossings
12
9
6
3
0
0
20
40
60
CT
3PO
Distance from soma (µm)
I
CT
3PO
J
10 Days
3 Months
HIF-1α
K
NeuN HIF-1α
GFAP HIF-1α
L
Number of crossings
12
9
6
3
0
0
20
40
60
WT
KO
Distance from soma (µm)
M
WT
HIF-1α KO

Figure 7

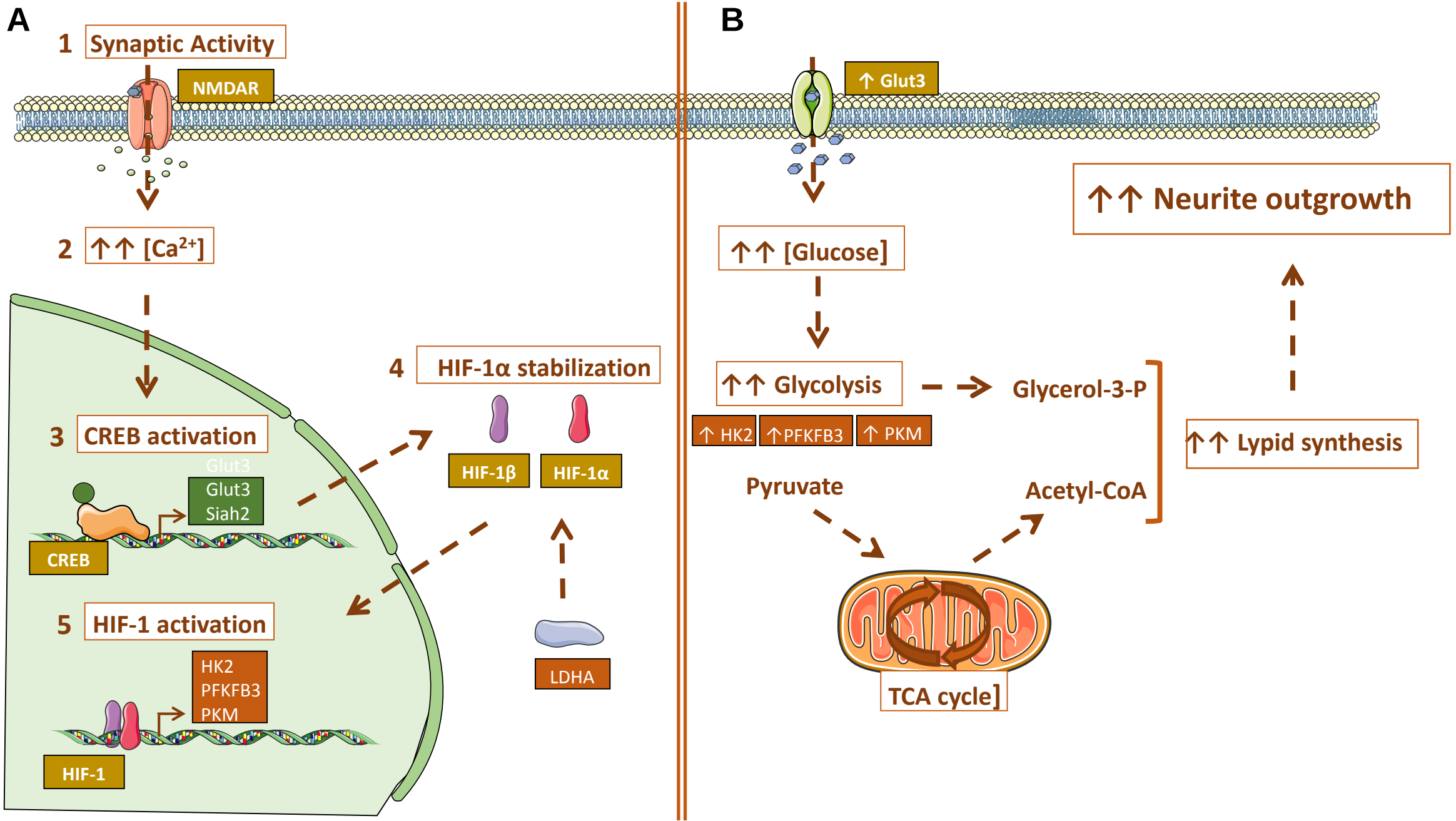
A
1 Synaptic Activity
NMDAR
2 ↑↑ [Ca2+]
3 CREB activation
Glut3
Glut3
Siah2
CREB
4 HIF-1α stabilization
HIF-1β
HIF-1α
5 HIF-1 activation
HK2
PFKFB3
PKM
HIF-1
LDHA
B
↑ Glut3
↑↑ Neurite outgrowth
↑↑ [Glucose]
↑↑ Glycolysis
↑ HK2
↑PFKFB3
↑ PKM
Glycerol-3-P
↑↑ Lypid synthesis
Pyruvate
Acetyl-CoA
TCA cycle]

Figure EV1 (related to figure 3)

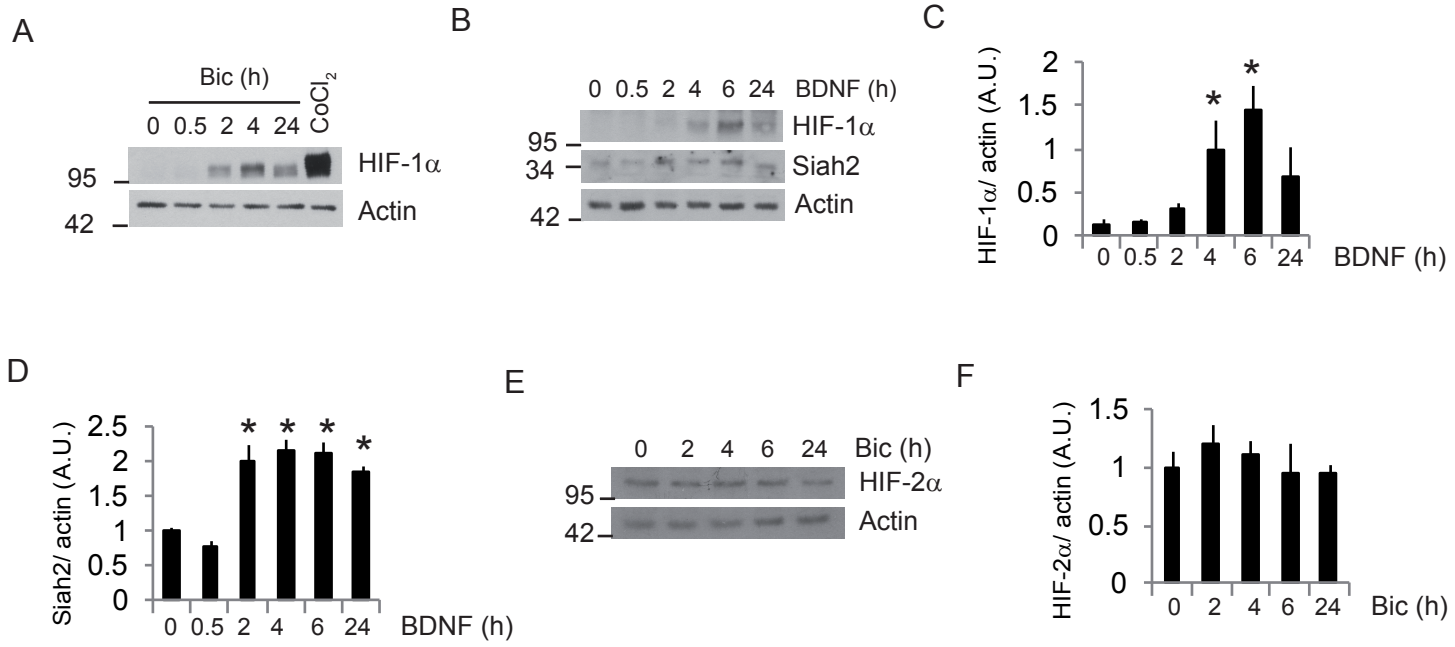

Figure EV1. Representative western blots of cortical neurons stimulated with (A) Bic+4-AP at the indicated time points or the hypoxia-mimetic $CoCl_2$ (200 μM) for 4 hours and (B) BDNF (25 ng/ml) for the indicated time points (n= 4-5 independent experiments) and (C and D) densitometric analysis. Values represent mean ± s.e.m. *p<0.05, two-tailed Student's t-test. E) Neurons were stimulated with Bic+4-AP for the indicated times and HIF-2α was analyzed by western blot. F) Densitometric analysis (n= 4 independent experiments). Values represent mean ± s.e.m.

Figure EV2 (related to figure 5)

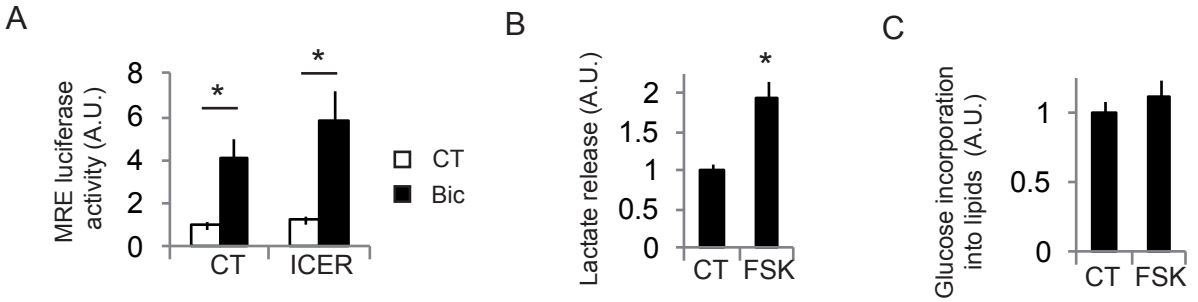

Figure EV2. A) Luciferase-based MEF2 activity in neurons expressing a control plasmid (globin) or a CREB inhibitor ICER and stimulated with Bic+4-AP for 8 hours (n= 7 independent experiments). Values represent mean ± s.e.m. *p<0.05, one-way ANOVA followed by Tukey's post-hoc test. B) Lactate released into the medium by neurons stimulated with 10 μM forskolin (for 24 h) (n= 4 independent experiments). Values represent mean ± s.e.m. *p<0.05, two-tailed Student's t-test. C) Lactate released into the medium by neurons stimulated with 10 μM forskolin (for 48 h) (n= 4 independent experiments).

Figure EV3 (related to figure 6)

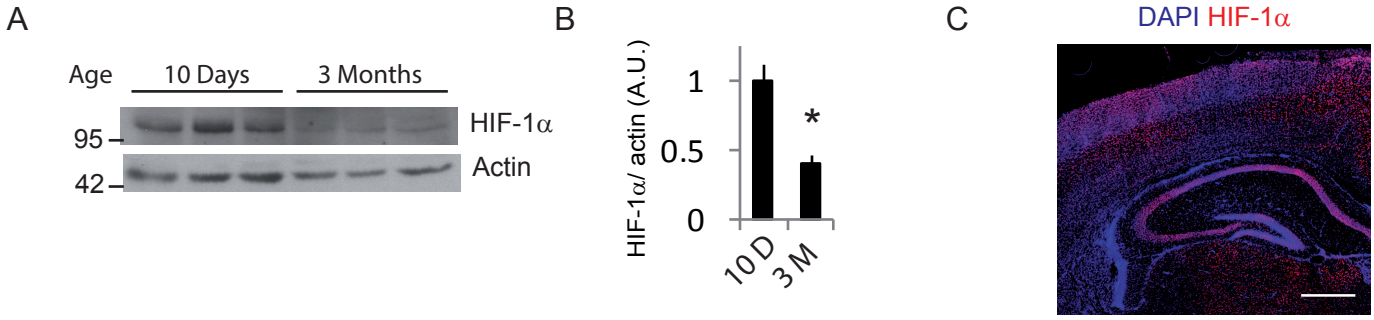

Figure EV3. A) Representative western blot of HIF-1α expression in protein extracts of the cortex of 10-day and 3-month old mice and (B) densitometric analysis (n= 4 mice per condition). Values represent mean ± s.e.m. *p<0.05, two-tailed Student's t-test. C) Immunfluorescence detection of HIF-1α in cortical sections from 10-day old mice (n= 3 mice per condition). Scale bar, 100 μm.

APPENDIX

Table of contents:

1. Appendix Supplementary Methods

Material and methods

Cell culture and stimulation

Cortical neurons from E21 Sprague Dawley rats were cultured as described previously (Martorell-Riera et al, 2015). Experiments were performed after a culturing period of 10–11 days during which cortical neurons develop a rich network of processes, express functional NMDA-type and AMPA/kainate-type glutamate receptors, and form synaptic contacts. Prior to stimulations and transfections, neurons were transferred from growth medium to a medium composed of 10% MEM (Invitrogen) and, 90% salt-glucose-glycine (SGG) medium (SGG: 114 mM NaCl, 0.219 % $NaHCO_3$, 5.292 mM KCl, 1 mM $MgCl_2$, 2 mM $CaCl_2$, 10 mM HEPES, 1 mM glycine, 30 mM glucose, 1 mM glutamine, 0.5 mM sodium pyruvate, 0.1% phenol red; osmolarity 325 mosm/l). Bursts of action potential firing were induced by treating of neurons with 50 µM bicuculline (Sigma), and burst frequency was enhanced by adding of 250 µM 4-amino pyridine (Sigma).

HIF-1α gene inactivation in vivo

To study the in vivo role of HIF-1α in neuronal architecture, we used previously described HIF1α floxed UBC-CRE-ERT2 mice (Soro-Arnaiz et al, 2016). These mice ubiquitously express a tamoxifen-inducible CRE recombinase (cre-ERT2) that allows global inactivation of HIF-1α locus flanked by two LoxP sites upon 4OH-tamoxifen treatment. For HIF-1α gene inactivation, the newborn mice received tamoxifen via breast feeding from the mother. Weaning mothers were injected intraperitoneally with 4OH-tamoxifen daily for 5 days (2 mg/day) starting 3-5 days postpartum. After this period females were returned to a standard mouse diet. Once newborns reached adulthood (4-6 months) neuronal architecture was analyzed. Mice were kept under specific pathogen-free conditions at the animal facility at the Autonomous University of Madrid (UAM).

3PO administration

P8 rat littermates were daily injected intraperitoneally for 5 days with 50 mg/kg PFKFB3 inhibitor 3PO (Merck) or DMSO (control). Six hours after the last injection, pups were sacrificed and brain was extracted to perform Golgi staining. Rats were kept under specific pathogen-free conditions at the animal facility at the Barcelona University (UB).

Histology

PFA-fixed brain mice (10-days and 3-months old) coronary sections (30 μm thicknes) were blocked for 2 hours at room temperature with PBS containing 10% of normal goat serum (NGS), 0.2% of gelatin. Anti-HIF-1α antibody (1:250) was incubated overnight at 4 °C with PBS-5% NGS. Sequential incubation with biotinylated anti-rabbit secondary antibody for 2 hours at room temperature (1:200; 711-065-152. Jackson Immunoresearch) followed with streptavidin-HRP incubation for 2 hours at room temperature temperature (1:400; Vectastain ABC kit, Vector Laboratories) was performed in PBS–5% NGS. Bound antibodies were visualized by

reaction using DAB and H_2O_2 as peroxidase substrates (Vectastain ABC kit, Vector Laboratories). Finally, sections were dehydrated and mounted.

For antigen immunodetection, sections were blocked for 2 h at RT with PBS-0.1% Triton-X-100 (PBST) containing 10% of fetal bovine serum (FBS), 0.2% of gelatin, and F(ab')2 fragment anti-mouse IgG (Jackson ImmunoResearch,1:300) when needed. Primary antibodies were incubated overnight at 4°C with PBS–5% FBS.

Anti-NeuN (Millipore) and anti-GFAP (DAKO) antibodies, dye-labeled secondary antibodies (1:300) were incubated for 2 h at RT in PBST–5% FBS. For the immunohistofluorescent detection of HIF1-α (Abcam), sequential incubation with biotinylated secondary antibodies in PBST–5% FBS (1:300; 2 h at 4ºC) and streptavidin-HRP (VECTASTAIN® Elite® ABC-HRP Kit, Vector Laboratories) (2 h at 4ºC) was performed . Bound antibodies were visualized by reaction using TSA® Plus Cyanine 3 detection kit (Perkin Elmer). Finally, sections were counterstained with DAPI (Sigma, 5 µm), mounted in Fluoromont and stored at −4°C.

For Golgi staining, impregnation was performed using Rapid Golgi Stain Kit (FD Neurotechnologies) following the manufacturer's protocol. Brains were stored in impregnation solution for two weeks in the dark. Coronal brain sections (150 µm thick) were obtained by slicing frozen brains with a cryostat, mounted in gelatin-coated slides and allowed to dry naturally at room temperature. Sections were then incubated during 10 minutes with staining solution, dehydrated and mounted with Eukitt (Sigma).

Transfection, plasmids and virus generation

Neurons were transfected at DIV8 using Lipofectamine 2000 (Invitrogen). Transfection efficiency was approximately 5 % which nearly the totality of transfected cells are neurons (Soriano et al, 2008). For knockdown experiments 25 ng of rat Glut3 (D-090091-01), rat ACLY

(M-098529-01-0005), rat Siah2 (L-089773-02) or non-targeting control (D-001810-10-05) siRNA-SMART pool (Thermo scientific) containing a pool of 4 siRNAs were used.

HRE-luciferase was a gift from Navdeep Chandel (Emerling et al, 2008) (Addgene plasmid # 26731); pCDNA3-HA-HIF-1α a gift from H Frankling Bunn (Huang et al, 1998); ODD-Luciferase-pcDNA3 (Addgene plasmid # 18965) and Luciferase-pcDNA3 (Addgene plasmid # 18964) were gifts from William Kaelin (Safran et al, 2006); CRE-luc and ICER were gifts from Giles Hardingham (Papadia et al, 2005).

The vectors used to construct and package recombinant adeno-associated viruses (rAAVs), pAAV-sh-sc, pAAV-GFP and pAAV-A-CREB were provided by Hilma Bading (Zhang et al, 2007). To construct pAAV-HIF-DN, the first 1,020 bp of the HIF-1α cDNA (from pCDNA3-HA-HIF-1α) were amplified using the following primers: forward 5'- AGA *GGA TCC* TAC CCA TAC GAT GTT CCA GAT -3' and reverse 5'- AAG CG*G ATA TC*T AAT TCA CAC ATA CAA TGC ACTG -3'. The amplified product contains sequences with BamHI and EcoRV restriction sites at the 5' and 3' respectively (italics). GFP in the rAAV-GFP vector was removed by BamHI/EcoRV digestion and the HIF-DN PCR product was cloned into the rAAV vector to express the first 340 amino acids of the HIF-1α N-terminus, which contains the DNA binding and dimerization domains, but not the ODD and transactivation domains. rAAV for shRNA expression contains the U6 promoter for shRNA expression and a CMV/chicken beta-actin hybrid promoter driving hrGFP expression. rAAV-shRNA was made by swapping the sh-sc sequence of rAAV-sh-sc for the following sequences of the rat gene into the BamHI and HindIII restriction sites: shSiah2(1): 5'-ACA GAG AAA CCA GAG CAT GAA -3'; shSiah2(2): 5'- GCA AGC AAG CAG AGA ACT TTG-3'; shGPI: 5'- GGA TTA CTC CAA GAA CCT TGT-3'; shACLY: 5'- GCA TCA AGC CTG GAT GCT TTA -3'. All newly generated constructs were confirmed by sequencing.

Neurons were infected with rAAV at DIV4. Infection efficiencies were determined at DIV 10-11 by analyzing GFP fluorescence or immunocytochemical analysis and were observed to range from 70 to 85% of the viable neurons.

Neurite length measurement

Cortical neurons were transfected with a plasmid expressing GFP and neurons were fixed 48 hours later with 4% paraformaldehyde, permeabilized, blocked and incubated over-night at 4°C with anti-GFP antibody (1:750, A11122, Life Technologies). Antibody binding was visualized using a biotinylated secondary antibody (1:200, Jackson Immuno Research) and Cy3-conjugated streptavidin (1:500, Jackson Immuno Research). Preparations were mounted on VECTASHIELD Mounting Medium with DAPI (Vector Laboratories).

Images were taken blindly at 4X magnification using an Olympus BX61 microscope equipped with an Olympus DP70 camera. Neurites were manually traced and analyzed using Simple Neurite Tracer software (Longair et al, 2011).

Luciferase assays

Cells were transfected with firefly luciferase-based reporter plasmid along with a Renilla expressing vector (pTK-RL; Promega), together with, where relevant, an HIF-DN or A-CREB expression vector. Luciferase assays were performed using the Dual Glo Luciferase Assay system (Promega) with firefly luciferase-based reporter gene activity normalized to the Renilla control (pTK-RL plasmid), except the CMV-ODD-Luc and CMV-Luc experiments that were normalized to CMV-Renilla.

RNA isolation, RT-PCR and qPCR

RNA was isolated using an PureLink™ RNA mini kit (Life Technologies). For qPCR, cDNA was synthesized from RNA using the SuperScript® III First-Strand Synthesis SuperMix (Life

Technologies) following the manufacturer's instructions. qPCR was performed in a StepOne Real-Time PCR System (Applied Biosystem) using GoTaq qPCR Master Mix (Promega) according to the manufacturer's instructions. The primers used were:

Glut3 -F: 5'- CAT CTC CGT TGT CCT CCA GT -3', -R: 5'- GCT CCA ATC GTG GCA TAG AT -3'; HK2 -F: 5'- CCA GCA GAA CAG CCT AGA CC -3, -R: 5'- AGA TGC CTT GAA TCC CTT TG -3'; PFK –F: 5'- CTG GGA GAG CGT GTC CAT-3', -R: 5'- CAT CGG GCA CTT CCA ATC -3'; PFKFB3 –F: 5'- ACA ATG AGG AGG CCA TGA GA -3', -R: 5'- CTT TGT CAG GTA GCT TTT GAC G -3'; PKM –F: 5'- GCC GCC TGG ACA TTG ACT C -3', -R: 5'- CCA TGA GAG AAA TTC AGC CGA G -3'; Siah2 –F: 5'- ATG CCG CCA GAA GTT GAG -3', -R: 5'- GTA TGG TGT AGA GTC AGG GAA CAG -3'; HIF-1α –F: 5'- AAC AGG ATG GAA TGG AGC AG -3', -R: 5'- TGG TCA GCT GTG GTA ATC CA -3'; GPI –F: 5'- AGT ACA TGC ACC GCT TTG CT-3', -R: 5'-ACT TTC CAT TGG ATT CCA TGT C-3'; Siah1 –F: 5'- TCTCCGCCCACAGAGATGAG -3', -R: 5'- GTTGGATGCAGTTGTGCCAG -3'; 18S -F: 5'-GTG GAG CGA TTT GTC TGG TT-3', -R: 5'-CAA GCT TAT GAC CCG CAC TT-3'. Expression of the gene of interest was normalized to that of 18S rRNA, a commonly used control.

Western blotting and antibodies

Mice cortices were frozen with liquid nitrogen and homogenized by pipetting and passing through a 29G syringe in a lysis buffer containing 50 mM HEPES, 150 mM NaCl, 1.5 mM MgCl 1mM EDTA, 1% Triton X-100, 1:00 Protease Inhibitor Cocktail Set III (EMD Milipore), 1:200 Phosphatase Inhibitor Cocktail II and III (Sigma) and 10 µM MG-132 (Sigma). Protein levels were quantified using Pierce BCA Protein Assay Kit (Thermo Scientific).

Total cell lysates were boiled at 100°C for 5 minutes in 1.5x sample buffer (1.5 M Tris pH 6.8; 15% Glycerol; 3% SDS; 7.5% β-mercaptoethanol; 0.0375% bromophenol blue). Gel electrophoresis was performed using 9% polyacrylamide gels. The gels were blotted onto PVDF membranes, that were then blocked for 1 hour at room temperature with 5% (w/v) non-fat dried milk in PBS with 0.05% Tween 20. The membranes were then incubated overnight at 4°C

with the primary antibodies diluted in blocking solution as follows: anti- Glut3 (1:750; ab191071, Abcam), PFKFB3 (1:1000, #13123, Cell Signaling Technology), PKM (1:750; #3190, Cell Signaling Technology), HK2 (1:500; sc-6521, Santa Cruz Biotechnology), HIF-1α (1:2000; ab179483, Abcam), Siah2 (1:350; sc-5507, Santa Cruz Biotechnology), Actin (1:10000, A4700, Sigma), FASN (1:500; sc-48357, Santa Cruz Biotechnology), ACLY (1:1000; #4332, Cell Signaling Technology), HIF2α (1:1000; ab179825, Abcam), PHD1 (1:1000; ab113077, Abcam); PHD2 (1:200; sc-271835, Santa Cruz Biotechnology), PHD3 (1:1000; NB100-139SS, Novus Biologicals), FIH-1 (1:500; sc-271780, Santa Cruz Biotechnology), OGDH (1:500; HPA020347, Sigma) and DLST (1:250; HPA003010, Sigma). To visualize western blots, HRP-based secondary antibodies were used followed by chemiluminescent detection on Kodak X-Omat film.

Acetyl-CoA and CoA determination

Acetyl-CoA and CoA levels were measured using the Acetyl-Coenzyme A and CoA Assay Kits, respectively (Sigma). Briefly, six well plates were used per condition (around 8 million neurons). Neurons were washed twice with PBS and scraped in PBS containing protease inhibitors (Inhibitor Cocktail Set III, EMD Millipore) and phosphatase inhibitors (Phosphatase Inhibitor Cocktail Set 1 and 3, Sigma). Neurons were pelleted, resuspended in 240 μl of lysis buffer (20 mM Tris pH 7.5, 150 mM NaCl, 1 mM EDTA, 1 mM EGTA, 1% Triton X-100, and protease and phosphatase inhibitors) and sonicated using a Diagenode Bioruptor (Liege, Belgium; 30 seconds on at full power and 30 seconds off, in an ice bath for 5 minutes). After centrifugation the supernatant was deproteinized using 10K Amicon-Ultra-0.5 mL centrifugal filters (EMD Millipore). Reaction mixtures in triplicate were set up according the kit's instructions.

To determine cytoplasmic acetyl-CoA levels, pelleted neurons were resuspended in ice-cold buffer containing 250 mM sucrose, 10 mM HEPES, pH 7.4, 1 mM EGTA, and protease and phospatase inhibitors. Neurons were homogenized using a Dounce homogenizer with a tight

fitting Teflon pestle (15 strokes). The homogenates were centrifuged at 14,000 *g* for 10 minutes and the supernatant deproteinized and assayed following the kit's instructions. Acetyl-CoA levels were normalized by total protein levels, quantified using Pierce BCA Protein Assay Kit (Thermo Scientific).

Glucose uptake measurements

The uptake of 2-[*N*-(7-nitrobenze-2-oxa-1, 3 diazol-4-yl) amino]-2 deoxy-glucose (2-NBDG, Life Technologies), a fluorescent glucose analog, was used to measure glucose transport. Cortical neurons were rinsed 3 times with phenol-red free SGG medium with reduced glucose concentration (0.5 mM) and incubated with 100 μM 2-NBDG in reduced glucose SGG medium for 30 minutes at 37ºC and 5% CO_2. Cultures were washed three times with phenol-red free SGG medium to remove free 2-NBDG. Accumulation of intracellular 2-NBDG, measured using an excitation wavelength of 488 nm, was imaged under a Leica DMIRB microscope equipped with a Leica DFC 550 camera at 40× magnification. ROIs of the same surface were drawn in the soma and fluorescence intensity was analyzed using ImageJ (Schneider et al, 2012).

Imaging studies

Neurons were visualized using a TCS SP2 Leica confocal laser scanning microscope (Leica Lasertechnick GmbH, Mannheim, Germany) adapted to an inverted Leitz DMIRBE microscope at 37°C in a controlled 5% CO2 atmosphere (Life Imaging Services). Pictures were acquired using a 40× (1.25-0.75 NA) Leitz Plan-Apochromatic objective. Images were analyzed using ImageJ software.

Cytoplasmic Ca^{2+} was monitored with Fluo-4 (Life Technologies). Neurons were loaded with 2 μM Fluo-4 for 45 min at room temperature in phenol-red free SGG medium with 10mM HEPES and 10mM glucose. After 3 washes with phenol-red free SGG medium, neurons were de-

esterified for 30 min at room temperature, excited at 488 nm and emission captured with a 516-nm filter.

For hypoxia analysis, neurons were loaded with 10 μM Image-IT Hypoxia Reagent (Life Technologies) in HBSS medium, and placed in an incubator chamber attached to the microscope, which was flushed with 95% N2/5% CO2 at a flow rate of 20 l/min at 37°C for 30min. Non-hypoxic neurons were maintained in normoxic conditions during probe incubation. Neurons were excited at 490 nm, and emission was measured using a 610-nm filter.

Lactate measurement

The culture medium was filtered using 10K Amicon Ultra-0.5 mL centrifugal filters (EMD Millipore). Then, 50 μL of medium was incubated with 200 μL of reaction buffer (320 mM glycine, 320 mM hydrazine, 2.4 mM NAD^+ and 2 U/mL of lactate dehydrogenase (LDH). After 30 minutes of incubation at room temperature, the lactate-dependent generation of NADH was measured at 340 nm using the Infinite 200 PRO multimode reader (Tecan). Lactate levels were normalized by total protein levels, quantified using Pierce BCA Protein Assay Kit (Thermo Scientific).

Glucose and glutamine incorporation into lipids

Neurons were grown on glass coverslips for 48 hours in a medium containing 0.8 μCi/ml ^{14}C-U-glucose (Perkin-Elmer) or 2 μCi/ml L-3-4-^{3}H(N)-glutamine (Perkin Elmer). Lipid isolation was performed as described previously by Folch et al. (Folch et al, 1957). Briefly, lipids were separated by submerging the coverslips in solution of methanol and chloroform 2:1 (vol:vol), and shaked for 20 minutes at room temperature. After adding one fifth of the volume of 0.154 M NaCl, the samples were centrifuged at 500 x g for 10 minutes at room temperature. 80% of the lower nonpolar phase containing the lipids was added to scintillation liquid and

desintigration per minute was determined by scintillation counting. The values were normalized by protein that was quantified from the polar phase using Pierce BCA Protein Assay Kit (Thermo Scientific).

ATP measurement

ATP levels were measured using the ATPlite Luminescence Assay System (Perkin-Elmer) on the Infinite 200 PRO multimode reader (TECAN) following the manufacteurer's instructions. ATP levels were normalized by total protein levels, quantified using Pierce BCA Protein Assay Kit (Thermo Scientific).

Statistical analysis

Statistical analysis involved two-tailed Student's t-tests. For any multiple comparisons within data sets, we used a one-way ANOVA followed by Tukey's post-hoc test. All data are presented as the mean ± s.e.m. of at least three independent experiments (n). A p value less than 0.05 was considered statistically significant.

2. Appendix Figures

Appendix Figure S1 (related to figure 1)

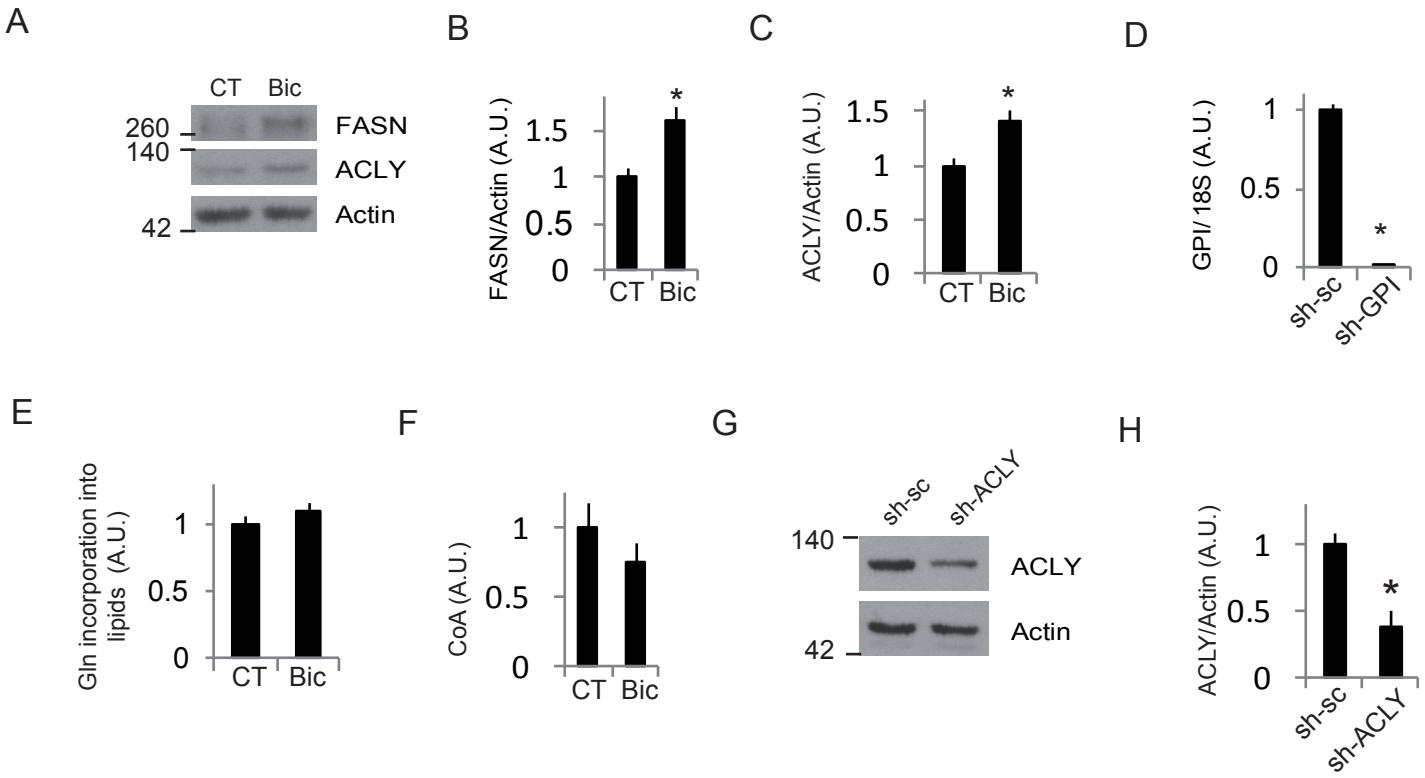

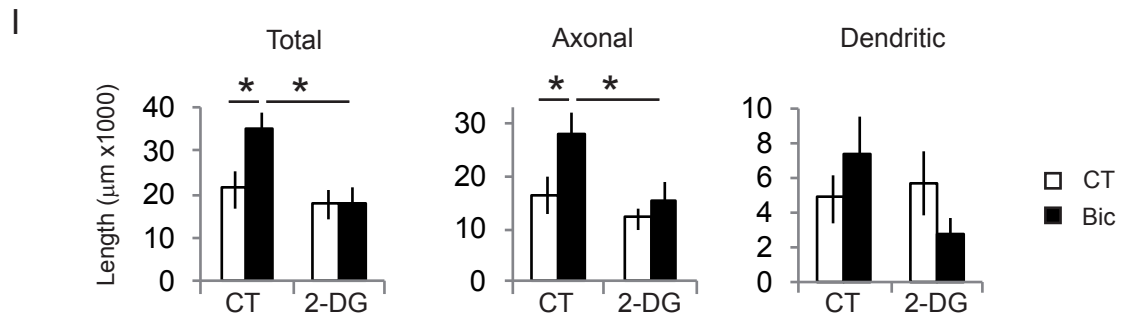

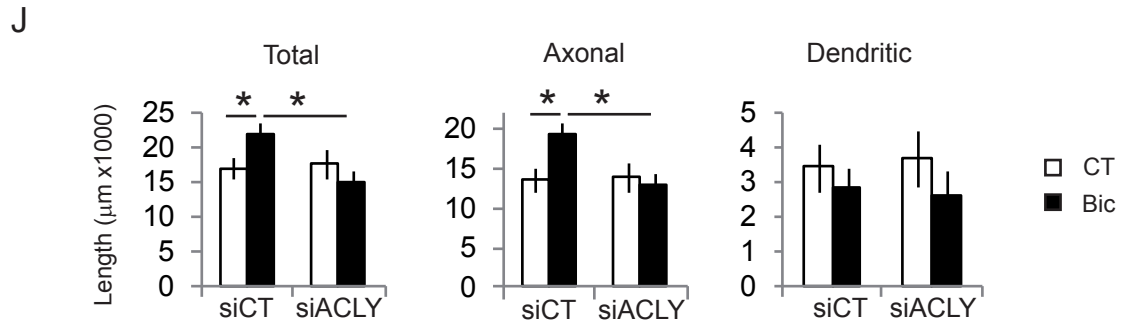

Appendix Figure S1. A) Cortical neurons were stimulated with Bic+4-AP for 4 hours and the indicated proteins were analyzed by western blotting. C and D) Densitometric analysis of the indicated proteins (n= 5 independent experiments). Values represent mean ± s.e.m. *p<0.05, two-tailed Student's t-test. E) GPI mRNA levels analyzed by qPCR of cortical neurons transduced with AAV expressing shRNA control (sh-sc) or targeting GPI (shGPI) (n= 4 independent experiments). Values represent mean ± s.e.m. *p<0.05, two-tailed Student's t-test. E) Neurons were incubated with ^{3}H-glutamine were stimulated with Bic+ 4-AP for 48 hours or left unstimulated (CT). Cellular lipids were extracted and radioactive counts measured (n= 4independent experiments). Values represent mean ± s.e.m. F) Determination of CoA levels after 24 hours Bic+4-AP stimulation (n= 4 independent experiments). Values represent mean ± s.e.m. G) Protein extracts of cortical neurons transduced with AAV expressing shRNA control (sh-sc) or targeting ACLY (shACLY) were analyzed by western blot and (H) densitometric analysis (n= 4 independent experiments). Values represent mean ± s.e.m. *p<0.05, two-tailed Student's t-test. I) Neurite length of control and Bic+4-AP stimulated neurons (for 48 hours) cultured in 25 mM of the non-metabolizable glucose analog 2-DG (n= 15 neurons from 3 independent experiments). Values represent mean ± s.e.m. *p<0.05, one-way ANOVA followed by Tukey's post-hoc test. J) Neurite length of control and Bic+4-AP stimulated neurons (for 48 hours) after transfection with non-targeting (siC) or ACLY-targeting (siACLY) siRNAs (n= 27-40 neurons from 6 independent experiments). Please, note that the siCT is the same that the shown in Fig. 6C since these experiments were done at the same time. Values represent mean ± s.e.m. *p<0.05, one-way ANOVA followed by Tukey's post-hoc test.

Appendix Figure S2 (related to figure 2)

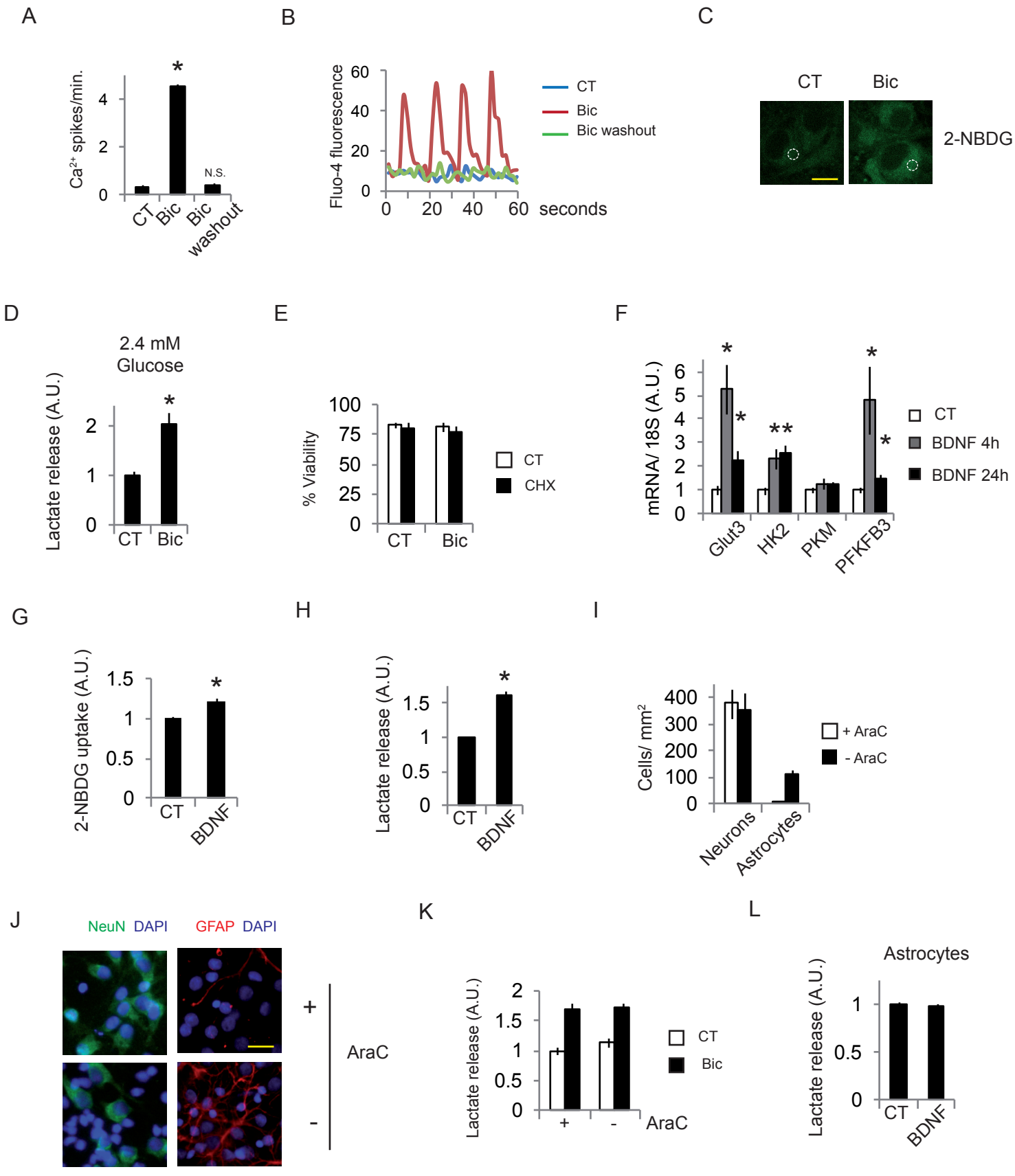

Appendix Figure S2. A) Fluo-4 determination of Ca2+ spikes in neurons unstimulated or stimulated for 1 minute or for 24 hours and washed for 30 minutes, to allow restoration of ionic gradients. B) Representative tracings. C) Representative images showing 2-NBDG uptake. The white circle represents a selected ROI to be analyzed. Scale bar, 5 μm. D) Lactate released into the medium by neurons stimulated with Bic+4-AP (for 24 h) in medium containing 2.4 mM glucose (n= 4 independent experiments). Values represent mean ± s.e.m. *p<0.05, two-tailed Student's t-test. E) Neuronal viability of neurons treated with cyclohexamide (10 μM) for 24 h. (n= 4 independent experiments). Values represent mean ± s.e.m. F) Cortical neurons were stimulated with BDNF (25 ng/ml) for 4 or 24 hours and mRNA expression of the indicated genes was determined by real-time qPCR (n= 3-6 independent experiments). Values represent mean ± s.e.m. *p<0.05, two-tailed Student's t-test. G) 2-NBDG uptake over 15 minutes in control or BDNF treated neurons (for 24 h) after washing and medium replacement (n= 4 independent experiments). Values represent mean ± s.e.m. *p<0.05, two-tailed Student's t-test. H) Neurons treated were stimulated with Bic+4-AP (for 24 h) before measuring the amount of lactate released into the medium (n= 4 independent experiments). Values represent mean ± s.e.m. *p<0.05, two-tailed Student's t-test. I) Quantification of glial and neuronal content in mixed cortical cultures treated or not with AraC (n= 3 independent experiments). Values represent mean ± s.e.m. J) Immunodetection of the indicated proteins in mixed cortical cultures treated or not with AraC. Scale bar, 25 μm. K) Lactate release after 24 hours of Bic+4-AP stimulation in mixed cultures with different proportions of astrocytes (n= 4 independent experiments). Values represent mean ± s.e.m. *p<0.05, one-way ANOVA followed by Tukey's post-hoc test. L) Lactate release in the medium of pure astrocyte culture treated for 24 hours with BDNF (25 ng/ml) (n= 3-7 independent experiments). Values represent mean ± s.e.m. *p<0.05, two-tailed Student's t-test

Appendix Figure S3 (related to figure 4)

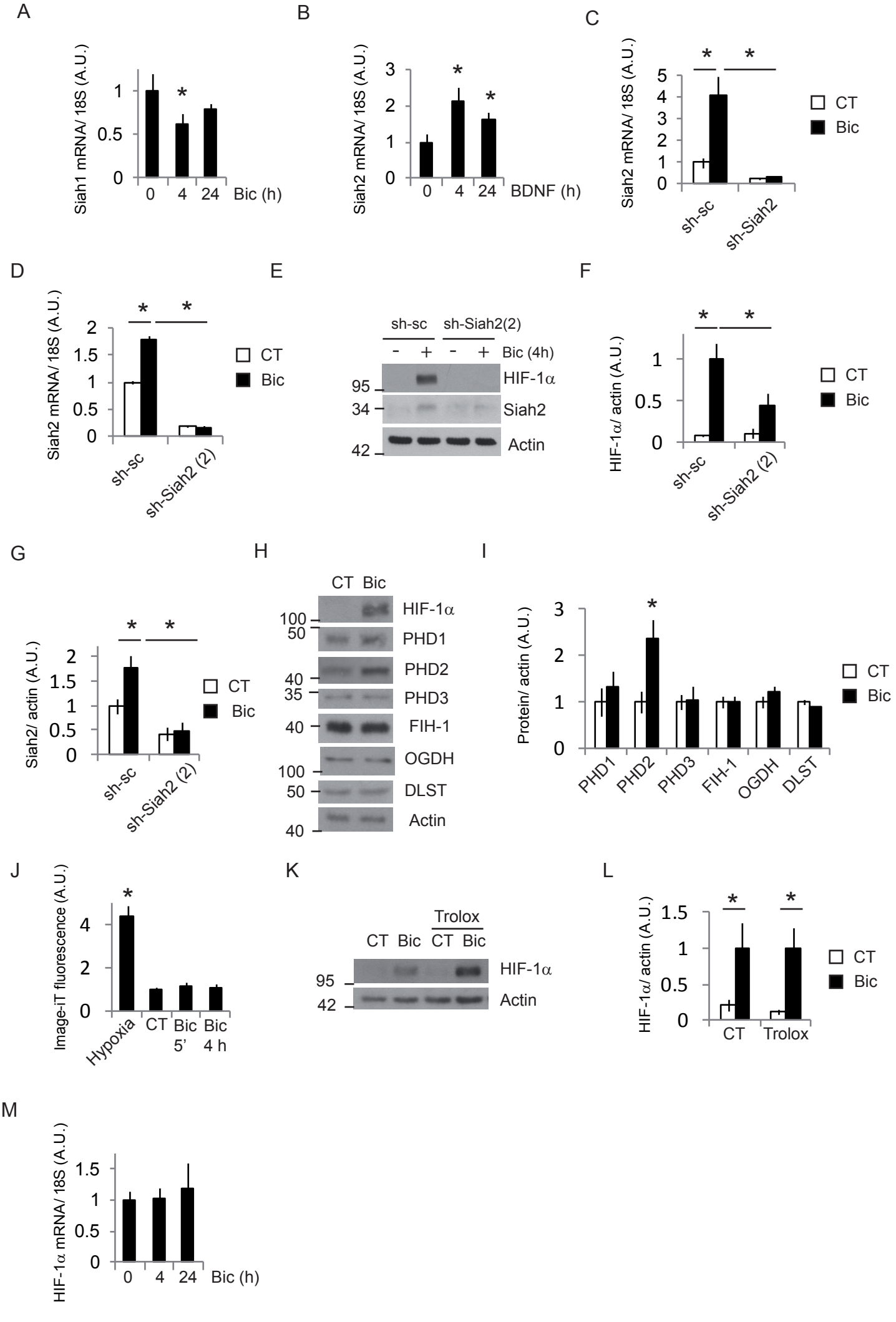

Appendix Figure S3. A) Neurons were stimulated with Bic+4-AP for the indicated times and Siah1 mRNA was analyzed by qPCR (n= 5 independent experiments). Values represent mean ± s.e.m., *p<0.05, two-tailed Student's t-test. B) Neurons were stimulated with BDNF (25 ng/mL) for the indicated times and Siah2 mRNA was analyzed by qPCR (n= 5 independent experiments). Values represent mean ± s.e.m., *p<0.05, two-tailed Student's t-test. C and D) Cortical neurons were transduced with AAV expressing non-targeting shRNA (sh-sc) or targeting Siah2 at two different sequences (sh-Siah2), stimulated for 4 hours with Bic+4-AP and the mRNA expression was analyzed by qPCR (n= 6 independent experiments). Values represent mean ± s.e.m. *p<0.05, one-way ANOVA followed by Tukey post-hoc test. E) Representative western blot and (F and G) densitometric analysis of the indicated proteins. Cortical neurons were transduced with AAV expressing non-targeting shRNA (sh-sc) or targeting Siah2 (sh-Siah2(2)) and stimulated for 4 hours with Bic+4-AP. (n= 4 independent experiments). Values represent mean ± s.e.m. *p<0.05, one-way ANOVA followed by Tukey post-hoc test. H) Representative western blot of the indicated proteins and (I) densitometric analysis of protein samples from control and Bic+4-AP-stimulated (24 hours) (n= 3-4 independent experiments). J) Analysis of Image-iT fluorescence of neurons subjected to hypoxia for 1 hour or in normoxia unstimulated (CT) or stimulated with Bic+4-AP for the indicated times(n= 3-7 independent experiments). Values represent mean ± s.e.m. *p<0.05, two-tailed Student's t-test. K) Representative western blot and (L) densitometric analysis of neurons stimulated for 4 hours with Bic+4-AP in absence or presence of 100 μM trolox. (n= 4 independent experiments). Values represent mean ± s.e.m. Synaptic activity does not causes increased HIF-1α mRNA expression. M) Neurons were stimulated with Bic+4-AP for the indicated times and HIF-1α mRNA was analyzed by qPCR (n= 3 independent experiments). Values represent mean ± s.e.m.